2018-01-10

Weakly nonlinear theory for oscillating wave surge converters in a channel

Michele, Simone

10.1017/jfm.2017.724
Journal of Fluid Mechanics
Cambridge University Press (CUP)

J. Fluid Mech. (2018), *vol.* 834, *pp.* 55–91.
doi:10.1017/jfm.2017.724

Weakly nonlinear theory for oscillating wave surge converters in a channel

S. Michele[1],†, **P. Sammarco**[1] **and M. d'Errico**[1]

[1]Department of Civil Engineering and Computer Science, Università degli Studi di Roma 'Tor Vergata', Via del Politecnico 1, 00133 Roma, Italy

(Received 15 July 2017; revised 20 September 2017; accepted 4 October 2017)

We present a weakly nonlinear theory on the natural modes' resonance of an array of oscillating wave surge converters (OWSCs) in a channel. We first derive the evolution equation of the Stuart–Landau type for the gate oscillations in uniform and modulated incident waves and then evaluate the nonlinear effects on the energy conversion performance of the array. We show that the gates are unstable to side-band perturbations so that a Benjamin–Feir instability similar to the case of Stokes' waves is possible. The non-autonomous dynamical system presents period doubling bifurcations and strange attractors. We also analyse the competition of two natural modes excited by one incident wave. For weak damping and power take-off coefficient, the dynamical effects on the generated power of the OWSCs are investigated. We show that the occurrence of subharmonic resonance significantly increases energy production.

Key words: general fluid mechanics, nonlinear dynamical systems, wave–structure interactions

1. Introduction

The surface-piercing flap-type oscillating wave surge converters (OWSCs) are among the most efficient devices to extract energy from water waves (Babarit *et al.* 2012). These devices consist of buoyant flaps hinged on a bottom foundation and move back and forth as an inverted pendulum under the action of the waves. A power take-off (PTO) mechanism converts the gate motion into electricity. Because of their ability to capture energy with large efficiency, these converters have received significant attention in recent years, leading to analytical theories (Linton & McIver 2001; Mei, Stiassnie & Yue 2005) and experimental campaigns (Folley, Whittaker & van't Hoff 2007; Henry *et al.* 2010). Renzi & Dias (2012, 2013, 2014) have developed a semi-analytical theory based on a hypersingular integral equation approach to investigate the hydrodynamic behaviour of a 'thin gate' in a channel and in open sea. Michele *et al.* (2015) and Michele, Sammarco & d'Errico (2016*a*) have extended the theory of Renzi & Dias (2013) to the case of a single and multiple arrays of neighbouring OWSCs with finite thickness in open sea and in front of a vertical breakwater. Recently, Michele, Sammarco & d'Errico (2016*b*) devised an analytical theory which describes the wave field and gate motion in terms of elliptic coordinates

† Email address for correspondence: michele@ing.uniroma2.it

and Mathieu functions, while Sarkar, Doherty & Dias (2016) solved the case of a finite array of cylindrical OWSCs.

The vast majority of existing analytical theories have been developed within the framework of linear theories for small amplitude oscillations. However, neglecting nonlinear effects is unjustified in some practical cases and might cause us to overlook constructive resonance phenomena. In this paper we describe a nonlinear theory for the hydrodynamic behaviour of a single array of several floating flap-gate OWSCs hinged on a fixed, rigid and fully reflecting wall. The gates oscillate under the action of the incident waves and an appropriate PTO located at the hinge converts the mechanical energy into electricity and returns a resistant torque. We consider the gates spanning the full width of an infinitely long channel. Due to the mirroring effect of the channel walls we thus model the behaviour of an infinite array of converters. In this case, the natural modes can be completely trapped with no radiation damping. Trapped modes are of considerable interest in several contexts such as acoustic waves (Hein & Koch 2008), quantum waveguides (Linton & Ratcliffe 2004), elastic waves (Porter 2007) and electromagnetic waves (Porter & Evans 1999). For water waves, Evans & Linton (1991) derived the wave field of trapped modes around a fixed vertical cylinder, while in coastal oceanography the wave trapping of edge waves on a sloping beach is well known (Blondeaux & Vittori 1995; Mei *et al.* 2005; Li 2007). In the case of neighbouring articulated gates Li & Mei (2003) developed a mathematical theory to determine all the out-of-phase trapped modes of an array of gates in an infinitely long channel; Sammarco, Michele & d'Errico (2013) solved the case of multiple arrays of gates hydrodynamically coupled.

Trapped modes cannot be synchronously resonated in a linearized framework. This is because the modal matrix and the forcing terms are orthogonal (Adamo & Mei 2005). For this reason, resonance of trapped modes is possible only through a nonlinear mechanism. Guza & Bowen (1976) and Rockliff (1978) have shown that trapped edge waves can be resonated subharmonically by incident waves with frequency twice the natural frequency of the edge wave. Li & Mei (2006) have developed a nonlinear theory to analyse the subharmonic resonance of trapped surface waves around a fixed cylinder while Lichter & Chen (1987) analysed the resonance of nonlinear cross-waves in a long channel. A similar subharmonic mechanism has been analysed for the so-called 'Faraday resonance': for the main contributions we refer to Miles (1984*a*), Holmes (1986), Gu & Sethna (1987) and Miles & Henderson (1990). Of considerable engineering interest is the case of mobile neighbouring gates to protect Venice from flooding. Laboratory experiments have revealed that, for certain frequencies, the incident waves resonate subharmonically the trapped modes of the barrier (Mei *et al.* 1994). The weakly nonlinear theory which explains this resonance mechanism has been developed by Sammarco, Tran & Mei (1997*a*), Sammarco *et al.* (1997*b*) for uniform and modulated waves. A simplified model for the subharmonic resonance of sliding gates in shallow waters has been developed by Vittori, Blondeaux & Seminara (1996).

In the present paper we extend the theory of Sammarco *et al.* (1997*a*,*b*) to investigate the hydrodynamics of the array of OWSCs. By considering small height of the gates with respect to the water depth, a simplified version of the governing equations and then for the coefficient of the evolution equation is found, with a new term that accounts for energy extraction. First, we consider subharmonic excitation of a single mode. We derive the complex nonlinear evolution equation of the Stuart–Landau form (Aranson & Kramer 2002) which describes the dynamical growth of the resonated trapped mode. A parametric analysis of the coupling coefficients

in terms of the array characteristics is carried out. The case of uniform incident waves points out the dependence of the bandwidth of instability, the resonated amplitude and the thresholds of resonance on the PTO coefficient. The generated power due to the subharmonic resonance of the natural modes is then evaluated. We find the optimal value of the PTO coefficient which maximizes power extraction and show that subharmonic excitation yields constructive interactions in terms of power extraction. We obtain that the capture factor is larger than the theoretical maximum of a two-dimensional absorber in a infinite long channel within the linear theory (Mei *et al.* 2005).

For modulated waves, we find period doubling sequences, chaotic states and frequency downshift (Trulsen & Mei 1995; Trulsen & Dysthe 1997; Sammarco *et al.* 1997*b*) by increasing the modulated wave amplitude. We detect the occurrence of homoclinic tangles and global chaos through usage of the Melnikov function (Guckenheimer & Holmes 1983; Jordan & Smith 2011). Extensive parametric analysis is then performed to study the effects of the chaotic behaviour on the generated power and efficiency. We show that chaotic motion of the gates decreases the efficiency in terms of energy production; a deterministic confirmation of the previous findings of Michele *et al.* (2016*a*,*b*) for gate energy production under stochastic incident wave spectra.

Next, we examine the competition of two modes assuming the incident wave frequency equal to the summation of the respective eigenfrequencies (Nayfeh & Mook 1995). Quadratic interactions at higher orders generate several harmonics. This nonlinear coupling leads to triad interactions and energy transfer between trapped modes. Interesting phenomena involving triad interactions have been studied in the context of acoustic–gravity waves (Kadri & Stiassnie 2013; Kadri & Akylas 2016), edge waves (Li 2007), Bragg scattering by bottom ripples (Mei *et al.* 2005) and interfacial waves (Alam 2012), while contributions to the analysis of mode–mode interactions can be found in Mei & Zhou (1991) and Zardi & Seminara (1995) for pulsating bubbles and Ciliberto & Gollub (1985), Simonelli & Gollub (1989), Kambe & Umeki (1990), Umeki (1991) for Faraday waves. The coupled evolution equations of both modal amplitudes are obtained and now involve coupling terms. Similarly to the case of single subharmonic resonance we derive the bifurcation diagrams to analyse the effects of the incident wave phase shift on the equilibrium and unstable states. The contribution due to mode–mode coupling on the OWSCs efficiency is finally given. We show that mode–mode coupling yields constructive interactions in terms of generated power but less pronounced than the pure subharmonic resonance of a single mode.

2. Governing equations

A sketch representing the array of floating OWSCs hinged upon a fixed, rigid and fully reflecting wall is depicted in figure 1. We indicate the physical variables by primes. The figure shows identical gates of width a' and thickness $2d'$ in an infinite straight long channel of width b'. Let h' and c' denote respectively the channel depth and the wall height; also $h'_p = h' - c'$ is the distance from the free surface to the hinge with $h'_p \ll h'$ (or $c' \sim h'$). Define a Cartesian reference system with the x' and y'-axes lying on the mean free surface and the z'-axis pointing vertically upward. The y'-axis bisects the array, while the x'-axis coincides with the left bank of the channel. The gates oscillate about a common axis located at $z' = -h' + c' = -h'_p$, $x' = 0$. Assume that the incoming waves come from $x \to +\infty$ and are normally incident to the gates. Let

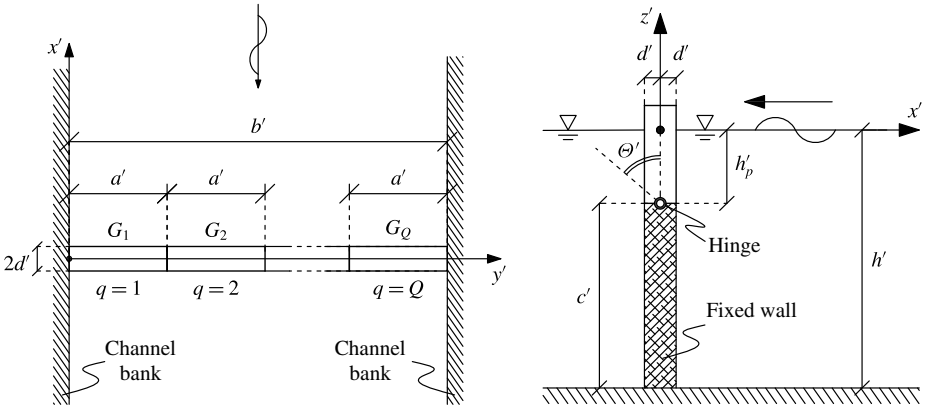

FIGURE 1. Plan geometry of the array and side view of the gate in physical variables. The OWSCs do not span the entire water depth but are placed upon a vertical fixed wall on a rigid bottom.

G_q, $q = 1, \ldots, Q$, denote the qth gate and Θ'_q be the angular displacement of G_q, then we can define $\Theta'(y, t) = \{\Theta'_1(t), \ldots, \Theta'_q(t), \ldots, \Theta'_Q(t)\}$ as the angular displacement function of the array. The fluid is assumed to be inviscid and incompressible and the flow irrotational, hence the velocity field satisfies the Laplace equation in the fluid domain Ω:

$$\nabla'^2 \Phi'(x', y', z') = 0 \quad (x', y', z') \in \Omega. \tag{2.1}$$

Let A'_T be the amplitude of the free-surface oscillations, λ' the wavelength, ω' the eigenfrequency of the natural mode and g' the acceleration due to gravity. Then introduce the following non-dimensional quantities:

$$\left.\begin{array}{c} (x, y, z) = (x', y', z')/\lambda', \quad \Phi = \Phi'/A'_T\omega'\lambda', \quad \zeta = \zeta'/A'_T, \quad t = t'\omega', \\ (b, c) = (b', c')/\lambda', \quad d = d'/h'_p, \quad h = h'/\lambda', \quad \Theta' = \Theta A'_T/h'_p, \quad G = g'/\omega'^2\lambda', \end{array}\right\} \tag{2.2}$$

where ζ' is the free-surface elevation and G the non-dimensional eigenfrequency. We introduce the following two length ratios to be smaller than unity:

$$\epsilon = A'_T/h'_p \ll 1, \quad \mu = h'_p/\lambda' \ll 1. \tag{2.3a,b}$$

With the introduction of these two small parameters the formulation of the problem becomes algebraically simpler to Sammarco *et al.* (1997*a*). Indeed, let Ω^+ (Ω^-) denote the fluid regions to the right (left) of the gates and distinguish physical quantities in $\Omega^\pm$ through $\pm$. Laplace and Bernoulli equations read

$$\nabla^2 \Phi^\pm = 0, \tag{2.4}$$

$$-\frac{p'^\pm}{\rho\omega'^2\lambda'^2} = Gz + \epsilon\mu\Phi_t^\pm + \epsilon^2\mu^2\frac{1}{2}|\nabla\Phi^\pm|^2, \tag{2.5}$$

the dynamic and mixed boundary condition on the free surface are respectively

$$-G\zeta = \Phi_t^\pm + \epsilon\mu\tfrac{1}{2}|\nabla\Phi^\pm|^2, \quad z = \epsilon\mu\zeta, \tag{2.6}$$

$$\Phi_{tt}^\pm + G\Phi_z^\pm + \epsilon\mu|\nabla\Phi^\pm|_t^2 + \epsilon^2\mu^2\tfrac{1}{2}\nabla\cdot\nabla|\nabla\Phi^\pm|^2 = 0, \quad z = \epsilon\mu\zeta, \tag{2.7}$$

while the no-flux conditions at the bottom and channel walls require

$$\Phi_z^{\pm} = 0, \quad z = -h, \tag{2.8a,b}$$

$$\Phi_y^{\pm} = 0, \quad y = 0 \quad \text{and} \quad y = b. \tag{2.9a–c}$$

The kinematic condition on the surface of the array

$$x = \xi^{\pm} = \left[-(z+\mu)\tan\epsilon\Theta \pm \mu \frac{d}{\cos^2\Theta} \right] H(z+h-c) \pm \mu\, dH(-z-h+c), \tag{2.10}$$

can be written as

$$\Phi_x^{\pm} = \left\{ \Theta_t \left[-\frac{(z+\mu)}{\mu\cos^2\epsilon\Theta} \pm \frac{d\sin\epsilon\Theta}{\cos^2\epsilon\Theta} \right] - \Phi_z^{\pm}\tan\epsilon\Theta \right\} H(z+h-c), \tag{2.11}$$

where H denotes the Heaviside step function.

Let us introduce a new pair of coordinates $(y_1, z_1) = (y', z')/h'_p = (y, z)/\mu$. The equation of motion of the qth gate coupled with an energy generator at the hinge is given by

$$\begin{aligned} &I\epsilon\Theta_{q,tt} - GS\sin\epsilon\Theta_q + \overline{\nu}_{pto}\epsilon\Theta_{q,t} \\ &\quad = -\int_{((q-1)a)/\mu}^{(qa)/\mu} \mathrm{d}y_1 \left\{ \int_{-1}^{\epsilon\zeta^+} \mathrm{d}z_1 \left(Gz_1 + \epsilon\Phi_t^+ + \epsilon^2\mu\frac{1}{2}|\nabla\Phi^+|^2 \right) \frac{z_1 + 1 - d\sin\epsilon\Theta_q}{\cos^2\epsilon\Theta_q} \right. \\ &\qquad \left. - \int_{-1}^{\epsilon\zeta^-} \mathrm{d}z_1 \left(Gz_1 + \epsilon\Phi_t^- + \epsilon^2\mu\frac{1}{2}|\nabla\Phi^-|^2 \right) \frac{z_1 + 1 + d\sin\epsilon\Theta_q}{\cos^2\epsilon\Theta_q} \right\} + O(\epsilon^4), \end{aligned} \tag{2.12}$$

where $I = I'/\rho h_p'^4\lambda'$ is the non-dimensional inertia of the gate about the hinge, $S = S'/\rho h_p'^4$ the non-dimensional first moment of the gate, $\overline{\nu}_{pto} = \nu'_{pto}/A_T^2\omega\rho h_p^2\lambda$ the non-dimensional power take-off coefficient. Typical values of ν'_{pto} are 10^2–10^3 kg m^2 s^{-1}, so that for typical conditions $A_T^2 = O(0.1)$ m, $\omega = O(1)$ rad s^{-1}, $h_p^2 = O(10)$ m, $\lambda = O(10)$–$O(10^2)$ m, we obtain $\overline{\nu}_{pto} = O(10^{-2})$. Hence we assume $\overline{\nu}_{pto} = \epsilon^2\nu_{pto}$. Note that usage of the coordinates (y_1, z_1) renders $O(1)$ the interval of the integrals in (2.12) and allows us to evaluate appropriately the order of magnitude of each term inside the integrand. Therefore, in the above expression (2.12) the contribution due to the PTO torque on the gate motion results small; indeed the term is $O(\epsilon^3)$. Hence, damping at $O(\epsilon)$ is purely hydrodynamical and depends on radiating waves towards infinity. Larger values of ν'_{pto} comparable with leading-order terms, i.e. $\overline{\nu}_{pto} = O(1)$, yield the equation of motion at $O(1)$ damped and unforced. Indeed, there are no forcing terms at this order because the incident wave is assumed to be at $O(\epsilon)$. Hence, we would obtain only synchronous motion at $O(\epsilon)$ and no subharmonic resonance.

Since the free-surface boundary conditions are given at $z = \mu\epsilon\zeta$, we perform Taylor expansion of (2.6) and (2.7) about $z = 0$:

$$-G\zeta = [\Phi_t^{\pm}]_{z=0} + \epsilon\mu[\Phi_{tz}^{\pm}]_{z=0}\zeta^{\pm} + \epsilon\mu[\tfrac{1}{2}|\nabla\Phi^{\pm}|^2]_{z=0} + O(\epsilon^3), \tag{2.13}$$

$$[\Phi_{tt}^{\pm} + G\Phi_z^{\pm}]_{z=0} + \epsilon\mu[\Phi_{ttz}^{\pm} + G\Phi_{zz}^{\pm}]_{z=0} + \epsilon\mu[|\nabla\Phi^{\pm}|_t^2]_{z=0} + O(\epsilon^3) = 0. \tag{2.14}$$

Similarly, Taylor expansion about $x = \pm\mu d$ of (2.10) and (2.11) yields

$$x = \xi^{\pm} = -(z+\mu)\epsilon\Theta H(z+h-c) + O(\epsilon^3), \tag{2.15}$$

$$\begin{aligned}[\Phi_x]_{x=x^{\pm}} \;=\; & -\Theta_t\frac{z+\mu}{\mu} + \epsilon\Theta(z+\mu)[\Phi_{xx}]_{x=x^{\pm}} - \epsilon^2\Theta^2(z+\mu)^2\left[\frac{\Phi_{xxx}}{2}\right]_{x=x^{\pm}} \\ & - \epsilon^2\Theta^2\Theta_t\frac{z+\mu}{\mu} - \epsilon\Theta[\Phi^{\pm}_z]_{x=x^{\pm}} + \epsilon^2\Theta^2(z+\mu)[\Phi^{\pm}_{zx}]_{x=x^{\pm}} \\ & \pm\epsilon\, d\Theta\Theta_t + O(\epsilon^3),\end{aligned} \tag{2.16}$$

where $x^{\pm} = \pm\mu d$ is a new variable. The equation of motion (2.12) becomes

$$\begin{aligned}& I\Theta_{q,tt} + GC\Theta_q + \epsilon^2\nu_{pto}\Theta_{q,t} + \epsilon^2 GS\frac{\Theta_q^3}{6} \\ & = -\int_{((q-1)a)/\mu}^{(qa)/\mu} \mathrm{d}y_1 \int_{-1}^{0} \mathrm{d}z_1 \Delta\Phi_t(z_1+1) - \epsilon\int_{((q-1)a)/\mu}^{(qa)/\mu} \mathrm{d}y_1 \left\{\frac{G\Delta\zeta^2}{2} + \Delta\Phi_t\zeta\right\} \\ & \quad - \epsilon^2\int_{((q-1)a)/\mu}^{(qa)/\mu} \mathrm{d}y_1 \int_{-1}^{0} \mathrm{d}z_1 \Delta\Phi_t\Theta^2(z_1+1) - \epsilon^2\int_{((q-1)a)/\mu}^{(qa)/\mu} \mathrm{d}y_1 \left\{\frac{G\Delta\zeta^3}{3} + \frac{\Delta\Phi_t\zeta^2}{2}\right\} \\ & \quad - \epsilon\mu\int_{((q-1)a)/\mu}^{(qa)/\mu} \mathrm{d}y_1 \int_{-1}^{0} \mathrm{d}z_1 \left\{-\Delta\Phi_{tx} + \frac{1}{2}\Delta|\nabla\Phi|^2(z_1+1)\right\} \\ & \quad + \epsilon\int_{((q-1)a)/\mu}^{(qa)/\mu} \mathrm{d}y_1 \int_{-1}^{0} \mathrm{d}z_1 2\, d\Theta\overline{\Phi_t} + \epsilon^2\int_{((q-1)a)/\mu}^{(qa)/\mu} \mathrm{d}y_1\, dG\Theta\overline{\zeta^2} + O(\epsilon^3),\end{aligned} \tag{2.17}$$

where $C = ad/\mu - S$ is the non-dimensional buoyancy restoring torque, while $\Delta(\cdot) = (\cdot)^{+}_{x=x^{+}} - (\cdot)^{-}_{x=x^{-}}$ and $\overline{(\cdot)} = [(\cdot)^{+}_{x=x^{+}} + (\cdot)^{-}_{x=x^{-}}]/2$ denote respectively the difference and the average of $(\cdot)$ on two sides of the array. A summary of the physical quantities as well as the dimensionless quantities is provided in tables 1 and 2.

3. Multiple-scale analysis

Let us introduce the following expansions of the non-dimensional velocity potential, free-surface elevation and gate oscillations:

$$\Phi^{\pm} = \Phi^{\pm}_1(x, y, z, t, t_2) + \epsilon\Phi^{\pm}_2(x, y, z, t, t_2) + \epsilon^2\Phi^{\pm}_3(x, y, z, t, t_2) + O(\epsilon^3), \tag{3.1}$$

$$\zeta^{\pm} = \zeta^{\pm}_1(x, y, t, t_2) + \epsilon\zeta^{\pm}_2(x, y, t, t_2) + \epsilon^2\zeta^{\pm}_3(x, y, t, t_2) + O(\epsilon^3), \tag{3.2}$$

$$\Theta^{\pm} = \Theta^{\pm}_1(y, t, t_2) + \epsilon\Theta^{\pm}_2(y, t, t_2) + \epsilon^2\Theta^{\pm}_3(y, t, t_2) + O(\epsilon^3), \tag{3.3}$$

where $t_2 = \epsilon^2 t$ denotes the slow time scale of the modal amplitude growth. Governing equation and boundary conditions yield for $n = 1, 2, 3$, the following equations.
Laplace equation:

$$\nabla^2\Phi^{\pm}_n = 0, \quad \text{in } \Omega^{\pm}. \tag{3.4}$$

Free-surface dynamic condition:

$$-G\zeta^{\pm}_n = \mathcal{B}_n, \quad z = 0, \tag{3.5a,b}$$

where

$$\mathcal{B}_1 = \Phi^{\pm}_{1_t}, \tag{3.6}$$

Parameters	Symbol	Dimensions
Time	t'	$[T]$
Physical coordinates	(x', y', z')	$[L]$
Acceleration due to gravity	g'	$[L][T]^{-2}$
Frequency	ω'	$[\text{rad}][T]^{-1}$
Pressure	p'	$[M][T]^{-2}[L]^{-1}$
Wavelength	λ'	$[L]$
Water density	ρ'	$[M][L]^{-3}$
Velocity potential	$\Phi'(x', y', z', t')$	$[L]^2[T]^{-1}$
Angular displacement	$\Theta'(y', t')$	$[\text{rad}]$
Free-surface elevation	$\zeta'(x', y', t')$	$[L]$
Channel depth	h'	$[L]$
Channel width	b'	$[L]$
Gate height	h'_p	$[L]$
Gate width	a'	$[L]$
Gate thickness	$2d'$	$[L]$
Wall height	c'	$[L]$
Gate inertia	I'	$[M][L]^2$
Gate first moment	S'	$[M][L]^2[T]^{-2}$
PTO coefficient	ν'_{pto}	$[M][L]^2[T]^{-1}$

TABLE 1. Physical parameters and their dimensions.

Dimensionless quantity	Symbol	Definition
Length ratio	ϵ	A'_T/h'_p
Length ratio	μ	h'_p/λ'
Time	t	$t'\omega'$
Physical coordinates	(x, y, z)	$(x', y', z')/\lambda'$
Strained physical coordinates	(y_1, z_1)	$(y', z')/h'_p$
Velocity potential	Φ	$\Phi'/A'_T\omega'\lambda'$
Angular displacement	Θ	Θ'/ϵ
Free-surface elevation	ζ	ζ'/A'_T
Channel depth	h	h'/λ'
Channel width	b	b'/λ'
Gate thickness	d	d'/h'_p
Gate width	a	a'/λ
Gate inertia	I	$I'/\rho h'^4_p\lambda'$
Gate first moment	S	$S'/\rho h'^4_p$
Gate buoyancy	C	$ad/\mu - S$
PTO coefficient	ν_{pto}	$\nu'_{pto}/A'^4_T\omega'\rho\lambda'$
Non-dimensional eigenfrequency	G	$g'/\omega'\lambda'$

TABLE 2. Dimensionless quantities.

$$\mathcal{B}_2 = \Phi^{\pm}_{2_t}, \tag{3.7}$$

$$\mathcal{B}_3 = \Phi^{\pm}_{3_t} + \Phi^{\pm}_{1_{tz}}\zeta_1^{\pm} + \tfrac{1}{2}|\nabla\Phi_1^{\pm}|^2 + \Phi^{\pm}_{1_{t_2}}. \tag{3.8}$$

Free-surface mixed condition:

$$\Phi^{\pm}_{n_{tt}} + G\Phi_{n_z} = \mathcal{F}_n, \quad z = 0, \tag{3.9}$$

where

$$\mathcal{F}_1 = 0, \tag{3.10}$$

$$\mathcal{F}_2 = 0, \tag{3.11}$$

$$\mathcal{F}_3 = -(\Phi^{\pm}_{1_{tt_z}} + G\Phi^{\pm}_{1_{zz}})\zeta_1^{\pm} - |\nabla\Phi^{\pm}_{1_t}|^2 - 2\Phi^{\pm}_{1_{tt_2}}. \tag{3.12}$$

No-flux boundary condition at the bottom:

$$\Phi_{n_z} = 0, \quad z = -h. \tag{3.13}$$

No-flux boundary condition on the channel walls:

$$\Phi_{n_y} = 0, \quad y = 0 \quad \text{and} \quad y = b. \tag{3.14a–c}$$

Kinematic condition on the array surface:

$$\Phi_{n_x} = \left(-\Theta_{n_t}\frac{z+\mu}{\mu} + \mathcal{G}_n\right) H(z+h-c), \quad x = x^{\pm}, \tag{3.15}$$

where

$$\mathcal{G}_1 = 0, \tag{3.16}$$

$$\mathcal{G}_2 = -\Phi^{\pm}_{1_z}\Theta_1 \pm d\Theta_1\Theta_{1_t}, \tag{3.17}$$

$$\begin{aligned}\mathcal{G}_3 \;=\; & \Phi^{\pm}_{1_{xx}}\Theta_1(z+\mu) - \Theta_{1_t}\Theta_1^2\frac{z+\mu}{\mu} - \Phi^{\pm}_{2_z}\Theta_1 - \Phi^{\pm}_{1_z}\Theta_2 \\ & - \Theta_{1_{t_2}}\frac{z+\mu}{\mu} \pm d(\Theta_1\Theta_2)_t.\end{aligned} \tag{3.18}$$

Equation of motion of the qth gate:

$$I\Theta_{q,n_{tt}} + GC\Theta_{q,n} = -\int_{((q-1)a)/\mu}^{(qa)/\mu} \mathrm{d}y_1 \int_{-1}^{0} \mathrm{d}z_1 \Delta\Phi^{\pm}_{n_t}(z_1+1) + \mathcal{D}_n, \tag{3.19}$$

where

$$\mathcal{D}_1 = 0, \tag{3.20}$$

$$\mathcal{D}_2 = -\int_{((q-1)a)/\mu}^{(qa)/\mu} \mathrm{d}y_1 \left\{G\frac{\Delta\zeta_1^2}{2} + \Delta\Phi_{1_t}\zeta_1\right\} + \int_{((q-1)a)/\mu}^{(qa)/\mu} \mathrm{d}y_1 \int_{-1}^{0} \mathrm{d}z_1 2d\Theta_1\overline{\Phi_{1_t}}, \tag{3.21}$$

$$\begin{aligned}\mathcal{D}_3 \;=\; & -\int_{((q-1)a)/\mu}^{(qa)/\mu} \mathrm{d}y_1 \int_{-1}^{0} \mathrm{d}z_1 \left\{\left[\Delta\Phi_{1_t}\Theta_1^2 - \frac{\mu}{\epsilon}\Delta\Phi_{1_{tx}}\Theta_2(z_1+1) + \frac{\mu}{\epsilon}\frac{1}{2}\Delta|\nabla\Phi_1|^2\right.\right. \\ & \left.\left. +\; \Delta\Phi_{1_{t_2}}\right](z_1+1)\right\} - \int_{((q-1)a)/\mu}^{(qa)/\mu} \mathrm{d}y_1 \left\{G\frac{\Delta\zeta^3}{3} + \frac{\Delta\Phi_{1_t}\zeta_1^2}{2} + G\Delta\zeta_1\zeta_2 + \Delta\Phi_{1_t}\zeta_2\right. \\ & \left. +\; \Delta\Phi_{2_t}\zeta_1\right\} - \nu_{pto}\Theta_{q,1_t} - 2I\Theta_{q,1_{tt_2}} + \int_{((q-1)a)/\mu}^{(qa)/\mu} \mathrm{d}y_1 \int_{-1}^{0} \mathrm{d}z_1 2\, d\{\Theta_1\overline{\Phi_{2_t}} + \Theta_2\overline{\Phi_{1_t}}\} \\ & \times \int_{((q-1)a)/\mu}^{(qa)/\mu} \mathrm{d}y_1\, dG\Theta_1\overline{\zeta_1^2} - \frac{GS}{6}\Theta^3_{q,1}.\end{aligned} \tag{3.22}$$

The latter forcing terms are algebraically simpler than those of Sammarco *et al.* (1997*a*). Indeed, the second-order boundary problem of Sammarco *et al.* (1997*a*) is forced on the free surface by the first-order solution. In the present case instead, the forcing term for the second-order free-surface mixed boundary condition $\mathcal{F}_2$ is null, as well as $\mathcal{F}_1$. This simplifies considerably the required algebra to seek the second-order solution because now the boundary conditions at $z=0$ and $z=-h$ are homogeneous and similar to those for the leading-order problem $O(1)$. Nevertheless, the dominant nonlinear effects are given by $\mathcal{G}_2$ (3.17) and $\mathcal{D}_2$ (3.21).

4. Subharmonic excitation of a single mode

It is known that an incident wave of frequency 2ω and amplitude $O(\epsilon)$ excites subharmonically a trapped mode of frequency ω of an array of floating gates (Mei *et al.* 1994; Sammarco *et al.* 1997*a*,*b*). A similar resonance mechanism is known in the context of edge waves. In this section we analyse the subharmonic resonance of a single trapped natural mode of an array of Q gates. Performing harmonic expansion of the governing equations, we obtain that the zeroth harmonic problem at the first and second order is unforced while the boundary value problem governing the first harmonic at the second order is identical to that governing the first harmonic at the first order (Sammarco *et al.* 1997*a*). For these reasons, we return in physical variables, omit the primes for brevity and assume the following solution:

$$\begin{aligned}\Phi^{\pm} &= \phi_1^{\pm}(x,y,z,t_2)\mathrm{e}^{-\mathrm{i}\omega t}+\epsilon\phi_2^{\pm}(x,y,z,t_2)\mathrm{e}^{-2\mathrm{i}\omega t}\\ &\quad+\epsilon^2\phi_3^{\pm}(x,y,z,t_2)\mathrm{e}^{-\mathrm{i}\omega t}+*+O(\epsilon^3),\end{aligned}\tag{4.1}$$

$$\zeta^{\pm}=\eta_1^{\pm}(x,y,t_2)\mathrm{e}^{-\mathrm{i}\omega t}+\epsilon\eta_2^{\pm}(x,y,t_2)\mathrm{e}^{-2\mathrm{i}\omega t}+\epsilon^2\eta_3^{\pm}(x,y,t_2)\mathrm{e}^{-\mathrm{i}\omega t}+*+O(\epsilon^3),\tag{4.2}$$

$$\Theta=\theta_1(y,t_2)\mathrm{e}^{-\mathrm{i}\omega t}+\epsilon\theta_2(y,t_2)\mathrm{e}^{-2\mathrm{i}\omega t}+\epsilon^2\theta_3(y,t_2)\mathrm{e}^{-\mathrm{i}\omega t}+*+O(\epsilon^3),\tag{4.3}$$

where $*$ denotes the complex conjugate and the second-order problem includes the harmonic 2ω only.

4.1. *Leading-order problem* $O(1)$

The $O(1)$ problem is homogeneous and unforced. Solution of the governing equations yields the well-known trapped natural modes of an array of Q gates in an infinitely long channel (Mei *et al.* 1994; Li & Mei 2003; Sammarco *et al.* 2013). The boundary value problem at the leading order is governed by the following equations:

$$\nabla^2\phi_1^{\pm}=0,\quad \text{in } \Omega^{\pm}\tag{4.4}$$

$$\phi_{1_z}^{\pm}=\phi_1^{\pm}\frac{\omega^2}{g},\quad z=0,\tag{4.5}$$

$$\eta_1^{\pm}=\frac{\mathrm{i}\omega}{g}\phi_1^{\pm},\quad z=0,\tag{4.6}$$

$$\phi_{1_x}^{\pm}=\mathrm{i}\omega\theta_1(z+h_p)H(z+h-c),\quad x=x^{\pm}.\tag{4.7}$$

By defining $\theta_1=\{r_{1q}\}\theta(t_2)$, with $\{r_{1q}\}=\{r_{11},\ldots,r_{1Q}\}$ the modal shape, we obtain the solution of the velocity potential,

$$\phi_1^{\pm}=\mp\mathrm{i}\theta\omega\sum_{q=1}^{Q}\sum_{m=1}^{\infty}\sum_{n=0}^{\infty}\frac{b_{mq}D_n}{C_n\alpha_{mn}}\mathrm{e}^{\mp\alpha_{mn}x}\cos\frac{m\pi y}{b}\cosh k_n(h+z)\equiv\mp\mathrm{i}\theta f_1^{\pm},\tag{4.8}$$

and of the free-surface elevation,

$$\eta_1^{\pm} = \pm \frac{\omega}{g} f_1^{\pm} \theta, \tag{4.9}$$

with k_n being the roots of the dispersion relation

$$\left.\begin{aligned} \omega^2 &= g k_0 \tanh k_0 h, \\ \omega^2 &= -g \bar{k}_n \tan \bar{k}_n h, \quad k_n = \mathrm{i}\bar{k}_n, \, n = 1, \ldots, \infty. \end{aligned}\right\} \tag{4.10}$$

The real coefficients b_{mq}, α_{mn}, C_n and D_n are defined by

$$b_{mq} = r_{1q} \frac{2}{m\pi} \left[\sin \frac{qm\pi}{Q} - \sin \frac{(q-1)m\pi}{Q} \right], \tag{4.11}$$

$$\alpha_{mn} = \sqrt{\left(\frac{m\pi}{b}\right)^2 - k_n^2}, \tag{4.12}$$

$$C_n = \frac{1}{2} \left(h + \frac{g}{\omega^2} \sinh^2 k_n h \right), \tag{4.13}$$

$$D_n = \frac{1}{k_n^2} [\cosh k_n c - \cosh k_n h + k_n (h - c) \sinh k_n h]. \tag{4.14}$$

Note that the real function $f_1^{\pm}$ defined in (4.8) has the properties

$$f_1^{+}(x) = f_1^{-}(-x), \quad f_{1_x}^{+}(x) = -f_{1_x}^{-}(-x), \tag{4.15a,b}$$

and that the wavenumber k_0 must satisfy the condition $k_0 < \pi/b$ in order that the absence/existence of propagating waves/trapped modes is satisfied.

Conservation of angular momentum for each gate G_j requires that

$$r_{1j}(-\omega^2 I + C) - \omega^2 I_j = 0, \tag{4.16}$$

where I_j is the added inertia defined as

$$I_j = \sum_{q=1}^{Q} \sum_{m=1}^{\infty} \sum_{n=0}^{\infty} \frac{2 b_{mq} b_{mj} D_n^2}{C_n \alpha_{mn}}, \tag{4.17}$$

with

$$b_{mj} = \frac{b}{m\pi} \left[\sin \frac{jm\pi}{Q} - \sin \frac{(j-1)m\pi}{Q} \right]. \tag{4.18}$$

As in Sammarco *et al.* (2013), solution of (4.16) yields $(Q-1)$ out-of-phase natural modes and related eigenfrequencies. The reader should refer to the work of Li & Mei (2003) for a complete list of modal shapes in which $2 \leqslant Q \leqslant 20$.

4.2. *The second-order problem* $O(\epsilon)$

Since the incident wave field is assumed to be at $O(\epsilon)$, the incident wave amplitude A' must be an order smaller than A'_T, thus $A'/A'_T = O(\epsilon)$. Hence, at $O(\epsilon)$ we assume the coexistence of the second harmonic 2ω with two components:

$$\phi_2^{\pm} = \phi_2^{\theta^{\pm}} + \phi^{A^{\pm}}, \tag{4.19}$$

where $\phi_2^{\theta^{\pm}}$ is the second-order potential forced by the quadratic products (3.17) on the gate surface, while $\phi^{A^{\pm}}$ is the second-order potential forced by the incident wave field.

4.2.1. *Radiated second harmonic* – $\phi_2^{\theta^\pm}$

The kinematic condition on the moving gates includes a forcing term,

$$\phi_{2_x}^{\theta^\pm} = \left[2\mathrm{i}\omega\theta_2^\theta(z+h_p) - \frac{\phi_{1_z}^\pm\theta_1}{\epsilon} \mp \mathrm{i}\omega\, d\frac{\theta_1^2}{\epsilon}\right] H(z+h-c), \quad x = x^\pm, \tag{4.20}$$

while the governing equation and the remaining boundary conditions on the free surface remain homogeneous like the $O(1)$ problem:

$$\nabla^2\phi_2^{\theta^\pm} = 0, \tag{4.21}$$

$$\phi_{2_z}^{\theta^\pm} = \frac{4\omega^2}{g}\phi_2^{\theta^\pm}, \quad z = 0, \tag{4.22}$$

$$\eta_2^{\theta^\pm} = \frac{2\mathrm{i}\omega}{g}\phi_2^{\theta^\pm}, \quad z = 0. \tag{4.23}$$

As the forcing term in (4.20) contains only the second harmonic, we assume the solution of the potential $\phi_2^{\theta^\pm}$ and of the angular motion θ_2 in the form

$$\phi_2^{\theta^\pm} = \mathrm{i}\theta^2 f_2^\pm, \quad \theta_2^\theta = \mathrm{i}\theta^2\theta_2. \tag{4.24a,b}$$

We get the following boundary value problem for the complex function $f_2^\pm$:

$$\nabla^2 f_2^\pm = 0, \tag{4.25}$$

$$f_{2_z}^\pm = \frac{4\omega^2}{g}f_2^\pm, \quad z = 0, \tag{4.26}$$

$$f_{2_x}^\pm = 2\mathrm{i}\omega\theta_2(z+h_p)H(z+h-c) \pm \frac{1}{\epsilon}\sum_{p=0}^{\infty}\Delta_p^\pm\cos\frac{p\pi y}{b}, \quad x = x^\pm, \tag{4.27}$$

where

$$\begin{aligned}\Delta_p^\pm &= \frac{\delta_p}{b}\int_0^b \mathrm{d}y(f_{1_z}^\pm r_{1q} - d\omega r_{1q}^2)\cos\frac{p\pi y}{b} \\ &= \frac{1}{2\delta_p}\sum_{q=1}^{Q}\left\{\sum_{m=1}^{\infty} b_{(m+p)q}\left[-d\omega b_{mq} + \sum_{n=0}^{\infty}\frac{\omega b_{mq}D_n}{C_n\alpha_{mn}}k_n\sinh k_n(h+z)\right]\right. \\ &\quad \left. + \sum_{m=1}^{\infty} b_{mq}\left[-d\omega b_{(m+p)q} + \sum_{n=0}^{\infty}\frac{\omega b_{(m+p)q}D_n}{C_n\alpha_{(m+p)n}}k_n\sinh k_n(h+z)\right]\right\}.\end{aligned} \tag{4.28}$$

Here δ_p denotes the Jacobi symbol, i.e. $\delta_0 = 1$ and $\delta_p = 2$, $p = 1, \ldots$. Note that the latter term is the same in both fluid regions: $\Delta_p^+ \equiv \Delta_p^-$.

Solution of the problem can be found by separation of variables:

$$f_2^\pm = -\mathrm{i}\sum_{p=0}^{\infty}\sum_{l=0}^{\infty}\frac{1}{\alpha_{pl}}\left(\frac{\Delta_{pl}}{\epsilon} \pm \sum_{q=1}^{Q}\frac{2\mathrm{i}b_{pq}\omega D_l}{C_l}\right)\mathrm{e}^{\pm\mathrm{i}\alpha_{pl}x}\cos\frac{p\pi y}{b}\cosh\kappa_l(h+z), \tag{4.29}$$

where

$$b_{mp} = r_{2q}\frac{2}{p\pi}\left[\sin\frac{qp\pi}{Q} - \sin\frac{(q-1)p\pi}{Q}\right], \tag{4.30}$$

κ_l are the real roots of the dispersion relation

$$\left.\begin{array}{c} 4\omega^2 = g\kappa_0 \tanh \kappa_0 h, \\ \kappa_l = \mathrm{i}\overline{\kappa}_l, \quad l = 1, \ldots, \infty, \\ 4\omega^2 = -g\overline{\kappa}_l \tan \overline{\kappa}_l h, \end{array}\right\} \tag{4.31}$$

while the coefficient Δ_{pl} is given by

$$\begin{aligned} \Delta_{pl} &= \frac{1}{C_l}\int_{-h}^{0} \mathrm{d}z \Delta_p \cosh \kappa_l (h+z) \\ &= \frac{1}{2\delta_p C_l}\sum_{q=1}^{Q}\sum_{m=1}^{\infty}\sum_{n=0}^{\infty}\left\{ b_{(m+p)q}\left[-d\omega b_{mq}E_l + \frac{\omega b_{mq} D_n C_{ln}}{C_n \alpha_{mn}}\right]\right. \\ &\quad \left. + b_{mq}\left[-d\omega b_{(m+p)q}E_l + \frac{\omega b_{(m+p)q} D_n C_{ln}}{C_n \alpha_{(m+p)n}}\right]\right\}, \end{aligned} \tag{4.32}$$

in which

$$\begin{aligned} C_{ln} &= \frac{1}{\kappa_l^2 - k_n^2}\left[\cosh k_n h \cosh \kappa_l h \left(\frac{4\omega^2}{g^2} - k_n^2\right)\right. \\ &\quad \left. + k_n^2 \cosh k_n c \cosh \kappa_l c - \kappa_l k_n \sinh k_n h \sinh \kappa_l h\right], \end{aligned} \tag{4.33}$$

$$E_l = \frac{1}{\kappa_l}(\sinh \kappa_l h - \sinh \kappa_l c). \tag{4.34}$$

Because of the symmetry properties (4.15), the equation of motion reads

$$r_{2j}(-4\omega^2 I + C) = 2\mathrm{i}\rho\omega \int_{(j-1)a}^{ja} \mathrm{d}y \int_{-h_p}^{0} \mathrm{i}\theta \Delta f_2(z + h_p)\, \mathrm{d}z, \tag{4.35}$$

however,

$$\Delta f_2 = \sum_{p=0}^{\infty}\sum_{l=0}^{\infty}\frac{4}{\alpha_{pl}}\sum_{q=1}^{Q}\frac{b_{pq}\omega D_l}{C_l}\cos\frac{p\pi y}{b}\cosh \kappa_l (h+z), \quad x = x^{\pm}, \tag{4.36}$$

so that substitution of the above expression in (4.35) yields a system of homogeneous equations in r_{2j}, $j = 1, 2$, with non-zero determinant of the coefficient matrix. As a result, the only solution is $r_{2q} = 0$, $q = 1, \ldots, Q$, i.e. the angular motion is zero. Finally, the complete solution of the second-order velocity potential forced by the trapped mode is

$$\phi_2^{\theta^{\pm}} = \theta^2 \sum_{p=0}^{\infty}\sum_{l=0}^{\infty}\frac{\Delta_{pl}}{\alpha_{pl}\epsilon}\mathrm{e}^{\pm \mathrm{i}\alpha_{pl}x}\cos\frac{p\pi y}{b}\cosh \kappa_l (h+z), \tag{4.37}$$

while the corresponding free-surface displacement is

$$\eta_2^{\theta^{\pm}} = -\frac{2\omega}{g} f_2^{\pm}\theta^2. \tag{4.38}$$

4.2.2. *Response to incident waves* – $\phi^{A^\pm}$

This is a simple diffraction problem where the incident wave field forces the gates to move at unison in phase. Decompose $\phi^{A^\pm}$ as follows:

$$\phi^{A^\pm} = \phi^I + \phi^S + \phi^{R^\pm}, \tag{4.39}$$

where

$$\phi^I = -\frac{\mathrm{i}Ag}{4\omega}\frac{\cosh\kappa_0(h+z)}{\cosh\kappa_0 h}\mathrm{e}^{-\mathrm{i}\kappa_0 x} \tag{4.40}$$

is the velocity potential of the incident waves of amplitude A,

$$\phi^S = -\frac{\mathrm{i}Ag}{4\omega}\frac{\cosh\kappa_0(h+z)}{\cosh\kappa_0 h}\mathrm{e}^{\mathrm{i}\kappa_0 x} \tag{4.41}$$

is the scattered wave potential, while

$$\phi^{R^\pm} = \pm\sum_{l=0}^{\infty}\frac{2\omega\theta^A D_l}{\kappa_l C_l}\cosh\kappa_0(h+z)\mathrm{e}^{\pm\mathrm{i}\kappa_0 x} \tag{4.42}$$

is the radiation potential. The angular response θ^A is given by

$$\theta^A = \frac{\rho a A g D_0/\cosh\kappa_0 h}{-4\omega^2 I + C - 8\mathrm{i}\omega^2\rho a\displaystyle\sum_{l=0}^{\infty}\frac{D_l^2}{\kappa_l C_l}}. \tag{4.43}$$

4.3. *The third-order problem* $O(\epsilon^2)$

At the order $O(\epsilon^2)$, the boundary conditions on the free surface and on the gate array surface are inhomogeneous. Since ω and ϕ_1 solve the homogeneous problem at the leading order we invoke the solvability condition applying Green's theorem to ϕ_1 and ϕ_3 over the entire fluid domain $\Omega^\pm$:

$$\iiint_{\Omega^\pm}(\phi_1^\pm\nabla^2\phi_3^\pm - \phi_3^\pm\nabla^2\phi_1^\pm)\,\mathrm{d}\Omega^\pm = \iint_{\partial\Omega^\pm}\left(\phi_1\frac{\partial\phi_3}{\partial n} - \phi_3\frac{\partial\phi_1}{\partial n}\right)\mathrm{d}S^\pm, \tag{4.44}$$

where the normal n points outward the volume boundaries $\partial\Omega$ and the volume integral on the left-hand side is null. Performing straightforward algebra we obtain

$$\begin{aligned} 0 \;=\; & \frac{\omega^2}{g}\int_0^b \mathrm{d}y\left(\int_{-\infty}^0 f_1^- \mathcal{F}_3^-\,\mathrm{d}x - \int_0^\infty f_1^+\mathcal{F}_3^+\,\mathrm{d}x\right) \\ & + 2\int_0^b \mathrm{d}y\int_{-h}^0 \overline{f_1\mathcal{G}_3}\,\mathrm{d}z + \sum_{q=1}^{Q}\frac{1}{\rho}\left(\mathrm{i}\mathcal{D}_3 r_{1q} - \frac{\nu_{pto}r_{1q}^2\omega\theta}{\epsilon^2}\right), \end{aligned} \tag{4.45}$$

where the forcing terms $\mathcal{F}_3$, $\mathcal{G}_3$, $\mathcal{D}_3$ are given by

$$\mathcal{F}_3^\pm = \pm\frac{2f_1^\pm\theta_t}{\omega}, \tag{4.46}$$

$$\begin{aligned} \mathcal{G}_3^\pm \;=\; & [-r_{1q}\theta^*(\mathrm{i}\theta^2 f_{2_z}^\pm + A\phi_z^{A^\pm}) \mp \mathrm{i}\theta^A f_{1_z}^\pm\theta^* - r_{1q}\theta_t(z+h_p) \\ & \pm d(\theta_1^*\theta_2)_t]\,H(z+h-c), \end{aligned} \tag{4.47}$$

$$\mathcal{D}_3^{\pm} = -\rho \int_{(q-1)a}^{qa} \mathrm{d}y \left\{ \int_{-h_p}^{0} f_1(-6r_{1q}^2\theta^*\theta^2\omega - 2\mathrm{i}\theta_t)(z+h_p)\,\mathrm{d}z + \frac{\omega^2 f_1}{g}\theta^* \left[-\frac{\omega f_1^2}{g}\theta^2 + 4h_p f_2\theta^2 - 4\mathrm{i}h_p\phi^D \right] \right\} + 2\omega I r_{1q}\mathrm{i}\theta_t - \frac{1}{2}gSr_{1q}^3\theta^2\theta^* - \rho\omega\, d\theta^* \int_{(q-1)a}^{qa} r_{1q}\,\mathrm{d}y \left\{ \int_{-h_p}^{0} (-4f_2\theta^2 + 2\mathrm{i}\phi^D)\,\mathrm{d}z - 3\omega\frac{f_1^2}{g}\theta^2 \right\}, \tag{4.48}$$

where $\phi^D = \phi^I + \phi^S$ is the diffraction potential and θ^* denotes the complex conjugate of θ. Solution of the integrals in (4.45) gives the evolution equation of the Stuart–Landau type:

$$-\mathrm{i}\theta_t = \theta^2\theta^*(c_N + \mathrm{i}c_R) + A\theta^* c_F + \mathrm{i}\theta\nu_{pto}c_L. \tag{4.49}$$

If there is a small detuning $2\Delta\omega$ such that $\Delta\omega/\omega \sim O(\epsilon^2)$, the above equation modifies as follows:

$$-\mathrm{i}\theta_t = \theta^2\theta^*(c_N + \mathrm{i}c_R) + A\mathrm{e}^{-2\mathrm{i}\Delta\omega t}\theta^* c_F + \mathrm{i}\theta\nu_{pto}c_L. \tag{4.50}$$

Through the transformation

$$\theta = \overline{\theta}\mathrm{e}^{-\mathrm{i}\Delta\omega t}, \tag{4.51}$$

equation (4.50) becomes

$$-\mathrm{i}\overline{\theta}_t = \Delta\omega\overline{\theta} + \overline{\theta}^2\overline{\theta}^*(c_N + \mathrm{i}c_R) + A\overline{\theta}^* c_F + \mathrm{i}\overline{\theta}\nu_{pto}c_L. \tag{4.52}$$

The coefficient c_N represents the shift of the trapped mode eigenfrequency from the incident wave frequency, c_R is the radiation damping due to wave radiation at $O(\epsilon)$, c_F represents the energy influx by the incident waves while c_L represents damping due to the PTO mechanism.

The coefficients of the evolution equation (4.52) c_L, c_F, $c_N + \mathrm{i}c_R$, are given respectively by

$$c_L = \frac{\omega}{c_T\rho}\sum_{q=1}^{Q} r_{1q}^2, \tag{4.53}$$

$$c_F = \frac{1}{\mathrm{i}c_T}\left(\int_0^b \mathrm{d}y \int_{-h_p}^{0} (-f_1 r_{1q}\phi_z^D + 2\omega\, dr_{1q}^2\phi^D)\,\mathrm{d}z - \int_0^b 2r_{1q}\omega^2 h_p\phi^D\frac{f_1}{g}\,\mathrm{d}y \right), \tag{4.54}$$

$$c_N + \mathrm{i}c_R = \frac{1}{c_T}\left\{ \int_0^b \mathrm{d}y \int_{-h_p}^{0} [-2\overline{f_1^{\pm} r_{1q} f_{2_z}^{\pm}} + 6\omega f_1 r_{1q}^3(z+h_p) - 4\mathrm{i}dr_{1q}^2 f_2\omega]\,\mathrm{d}z + \int_0^b r_{1q}\omega^2\left(\omega\frac{f_1^3}{g^2} - 4h_p\frac{f_1}{g}f_2 + 3dr_{1q}\frac{f_1^2}{g}\right)\mathrm{d}y - \frac{gSr_{1q}^4}{2\rho} \right\}, \tag{4.55}$$

with

$$c_T = \frac{4\omega}{g}\int_0^b \mathrm{d}y \int_0^{\infty} f_1^2\,\mathrm{d}x + 2\int_0^b \mathrm{d}y \int_{-h_p}^{0} f_1 r_{1q}(z+h_p)\,\mathrm{d}z + \sum_{q=1}^{Q} 2I\omega r_{1q}^2. \tag{4.56}$$

Computation of c_F, c_N, c_R and c_T can be evaluated by numerical calculation of the integrals with the known expressions of the integrands.

4.4. *Dynamical system analysis for uniform incident waves*

By making use of action-angle variables R and ψ expressed by $\overline{\theta} = \mathrm{i}\sqrt{R}\mathrm{e}^{\mathrm{i}\psi}$ we obtain the following autonomous dynamical system in R and ψ:

$$\left.\begin{array}{c} R_t = -2R(-2c_R R + c_F A \sin 2\psi + c_L \nu_{pto}) \\ \psi_t = \Delta\omega + c_N R - c_F A \cos 2\psi. \end{array}\right\} \tag{4.57}$$

With the requirement $R_t = 0$, $\psi_t = 0$ we find at least three fixed points. The trivial fixed point is located at

$$R = 0, \quad \psi = (1/2)\cos^{-1}\frac{\Delta\omega}{c_F A} = \psi^*. \tag{4.58a,b}$$

It is easily shown that this point is an unstable saddle for $|\Delta\omega| < \sqrt{A^2 c_F^2 - \nu_{pto}^2 c_L^2}$, and a stable fixed point otherwise. The latter condition fixes the threshold of resonance,

$$A > \frac{c_L}{c_F}\nu_{pto}, \tag{4.59}$$

i.e. for large values of the PTO coefficient ν_{pto} there is no subharmonic resonance from the rest position and only in-phase motion occurs. Now we seek the non-trivial fixed points which correspond to the roots of the quadratic equation:

$$R^2(c_N^2 + c_R^2) + 2R(c_R \nu_{pto} c_L + \Delta\omega c_N) + \nu_{pto}^2 c_L^2 + \Delta\omega^2 - A^2 c_F^2 = 0, \tag{4.60}$$

i.e.

$$R^{\pm} = \frac{-\nu_{pto} c_L c_R - c_N \Delta\omega \pm \sqrt{A c_F^2 (c_N^2 + c_R^2) - \nu_{pto} c_L c_N + c_R \Delta\omega}}{c_N^2 + c_R^2}. \tag{4.61}$$

The latter corresponds to two branches of an ellipse in the plane $\Delta\omega, R$. Since the square root of (4.61) must be real and $R^{\pm} > 0$, we obtain a single non-trivial fixed point R^+ for

$$-\sqrt{A^2 c_F^2 - \nu_{pto}^2 c_L^2} < \Delta\omega < \sqrt{A^2 c_F^2 - \nu_{pto}^2 c_L^2}, \tag{4.62}$$

and the coexistence of two non-trivial fixed points $R^{\pm}$ for

$$\frac{\nu_{pto} c_L c_N - A c_F \sqrt{c_N^2 + c_R^2}}{c_R} < \Delta\omega < -\sqrt{A^2 c_F^2 - \nu_{pto}^2 c_L^2}. \tag{4.63}$$

The latter holds if

$$\nu_{pto} < \frac{c_N A c_F}{c_L \sqrt{c_N^2 + c_R^2}}, \tag{4.64}$$

this is because ν_{pto} alters the threshold of instability and determines the vanishing of R^-. Analysis of the Jacobian matrix at the fixed points reveals that R^+ is stable while R^- correspond to an unstable saddle. It is worth evaluating the maximum value of the equilibrium amplitude which corresponds to the maximum of the stable state R^+. Taking the derivative of R^+ with respect to $\Delta\omega$ we obtain

$$R_{max} = \frac{A c_F - \nu_{pto} c_L}{c_R}, \quad \text{at } \Delta\omega_{max} = \frac{c_N(\nu_{pto} c_L - A c_F)}{c_R}, \tag{4.65a,b}$$

or in terms of the modal amplitude:

$$|\overline{\theta}|_{max} = \sqrt{\frac{Ac_F - \nu_{pto} c_L}{c_R}}. \tag{4.66}$$

Once $|\overline{\theta}|$ is evaluated, the average generated power by the array due to subharmonic resonance of the natural mode is given by

$$P_s(\nu_{pto}, R^+) = \frac{\omega}{2\pi} \int_0^{2\pi/\omega} \nu_{pto} \sum_{q=1}^{Q} \left(\frac{\mathrm{d}\Theta_q}{\mathrm{d}t} \right)^2 \mathrm{d}t = 2\nu_{pto} (\omega + \Delta\omega)^2 \sum_{q=1}^{Q} r_{1q}^2 R^+. \tag{4.67}$$

The maximum of P_s depends on $\Delta\omega$ and ν_{pto} and cannot be found analytically. Numerical calculation of (4.67) reveals that a good approximation consists in finding the optimal value of ν_{pto} which maximizes the generated power at $\Delta\omega = \Delta\omega_{max}$ where the gate oscillation is maximum. So we impose the derivative of (4.67) with respect to ν_{pto} evaluated at $\Delta\omega_{max}$ to be zero:

$$\left. \frac{\mathrm{d}P_s}{\mathrm{d}\nu_{pto}} \right|_{\Delta\omega = \Delta\omega_{max}} = 0. \tag{4.68}$$

Solution of the latter equation yields a criterion to find the optimal value of the PTO coefficient which maximizes the power output:

$$\nu_{pto} = \frac{c_T \rho}{8 c_N \omega \sum_{q=1}^{Q} r_{1q}^2} \left(5Ac_F c_N - 2c_R \omega + \sqrt{9A^2 c_F^2 c_N^2 - 4Ac_F c_N c_R \omega + 4c_R^2 \omega^2} \right). \tag{4.69}$$

Finally we assess the maximum efficiency of the system by considering the capture width ratio $\mathcal{C}^F$ (Mei *et al.* 2005) defined as the ratio between P_s and the incident wave energy flux per array width b (Michele *et al.* 2016*b*):

$$\mathcal{C}^F = \frac{P_s}{EC_g b}, \tag{4.70}$$

where

$$EC_G = \frac{\rho g A^2 (\omega + \Delta\omega)}{2k} \left(1 + \frac{2kh}{\sinh 2kh} \right). \tag{4.71}$$

In the latter, C_G is the group velocity and k the wavenumber related to the frequency $2(\omega + \Delta\omega)$.

4.5. *The non-autonomous dynamical system for modulated incident waves*

In this section we investigate the effects of a modulation of the incident wave envelope on the dynamics and power generated by the array. Let us assume

$$A = \overline{A} + \tilde{A} \cos \Omega t, \tag{4.72}$$

where $\overline{A}$ is the constant amplitude of the short waves, while $\tilde{A}$ and Ω are respectively the amplitude and frequency of the modulation with order $O(\epsilon^2)$. The evolution equation now includes a forcing term in time and becomes

$$-\mathrm{i}\overline{\theta}_t = \Delta\omega\overline{\theta} + \overline{\theta}^2\overline{\theta}^*(c_N + \mathrm{i}c_R) + (\overline{A} + \tilde{A}\cos\Omega t)\overline{\theta}^* c_F + \mathrm{i}\overline{\theta}c_L. \tag{4.73}$$

In action-angle coordinates the latter equation reads

$$\left.\begin{aligned} R_t &= -2R[-2Rc_R + (\overline{A} + \tilde{A}\cos\Omega t)c_F \sin 2\psi + c_L] \\ \psi_t &= \Delta\omega + Rc_N - (\overline{A} + \tilde{A}\cos\Omega t)c_F\cos 2\psi. \end{aligned}\right\} \tag{4.74}$$

The latter non-autonomous system is similar to that for Venice gates (Sammarco *et al.* 1997*b*) and can exhibit chaos for a certain range of the long wave amplitude $\tilde{A}$. There are different theoretical criteria to determine under what conditions the response of a dynamical system becomes chaotic. In this paper we make use of the Melnikov method. This mathematical technique allows us to predict global chaos and is based on the search of horseshoe maps and homoclinic/heteroclinic orbits of the associated undamped Hamiltonian system (Guckenheimer & Holmes 1983). Let us assume the following variables:

$$\left.\begin{gathered} \alpha = \frac{c_N}{c_R}, \quad \beta = \frac{c_L}{\overline{A}c_F}, \quad W = \frac{\Delta\omega}{\overline{A}c_F}, \quad \vartheta = \sqrt{\frac{c_N}{\overline{A}c_F}}\theta, \\ T = \overline{A}c_F t, \quad a = \frac{\tilde{A}}{\overline{A}}, \quad \sigma = \frac{\Omega}{c_F\overline{A}}, \end{gathered}\right\} \tag{4.75}$$

and the damping and forcing terms to be $O(\delta)$ with $\delta \ll 1$. By denoting with $\vartheta = \mathrm{i}\sqrt{R'}\mathrm{e}^{\mathrm{i}\psi'}$, the system (4.74) can be rewritten in the form

$$\left.\begin{aligned} R'_t &= -2R\sin 2\psi' - 2R'\delta(\alpha R' + a\sin 2\psi'\cos\sigma T + \beta) \\ \psi'_t &= W + R' - \cos 2\psi' - \delta a\cos 2\psi'\cos\sigma T. \end{aligned}\right\} \tag{4.76}$$

The Hamiltonian function of the unforced system is then given by

$$H = \frac{R'^2}{2} - R'\cos 2\psi' + WR'. \tag{4.77}$$

At $O(1)$ the system (4.76) admits three fixed points:

$$O = \{0, \tfrac{1}{2}\cos^{-1} W\}, \quad s = \{1 - W, 0\}, \quad u = \{-1 - W, 0\}, \tag{4.78a–c}$$

where O is an unstable saddle for $|W| < 1$ and a centre if $|W| > 1$, the fixed point s is a centre and exist for $W < 1$ while u is an unstable saddle and exist for $W < -1$. Because heteroclinic tangle is difficult to excite experimentally (Sammarco *et al.* 1997*b*), we focus our attention to the bifurcation of homoclinic paths assuming $W = 0$. In this case the homoclinic orbit has the equation

$$R^h = \frac{2}{\cosh 2(T - T_0)}, \quad \psi^h = \tan^{-1}\{\tanh(T - T_0)\}, \tag{4.79a,b}$$

and the corresponding Melnikov function is given by

$$M(T_0) = \int_{-\infty}^{\infty} 2R^h[a_1 R^h \sin 2\psi^h \cos\sigma T + (R^h - \cos 2\psi^h)(\alpha_1 R^h + \beta_1)]\,\mathrm{d}T, \tag{4.80}$$

Parameters	Symbol	Value (m)
Water depth	h'	15
Wall height	c'	12.5
Gate width	a'	1
Gate thickness	d'	0.3

TABLE 3. Flap and channel dimensions.

where

$$(\alpha_1, \beta_1, a1) = \frac{(\alpha, \beta, a)}{\mu}. \tag{4.81}$$

Homoclinic tangle occurs when $M(T_0)$ has a simple zero. The integral (4.80) can be evaluated analytically, and gives the lower threshold in terms of the modulated amplitude $\tilde{A}$ to give rise to horseshoe structures in the neighbourhood of the homoclinic orbit R^h, ψ^h:

$$\tilde{A} = \frac{4\overline{A}^3 c_F^2}{\pi \Omega^2} \left(\frac{\pi c_R}{c_N} + \frac{2c_L}{\overline{A} c_F} \right) \sinh \frac{\pi \Omega}{4\overline{A} c_F}. \tag{4.82}$$

Note that the smaller the damping due to $O(\epsilon)$ radiated waves and PTO coefficient, the lower is the threshold. Moreover, taking the limit of (4.82) for $\Omega \to (0, \infty)$ we obtain that $\tilde{A}$ tends to infinity and chaos is not generated.

4.6. *Results for uniform incident waves and* $Q = 2$

Here we discuss the theoretical results of the previous section for the case of $Q = 2$ gates with channel and array dimensions listed in table 3. Let us assume the amplitude of the incident wave $A = 0.1$ m. Solution of the $O(1)$ problem yields a trapped mode with eigenvector $r_{1q} = \{1, -1\}$. The values of the coefficients c_L, c_N, c_R and c_F with respect to the eigenfrequency ω are shown in figure 2. All the coefficients show similar behaviour, i.e. they increase with the eigenfrequency of the mode.

In figure 3 we show the dependence of the maximum value of the capture factor $\mathcal{C}^F_{max}$ (4.70) and of the optimal value of the PTO coefficient (4.69) on the eigenfrequency ω. The larger the eigenfrequency the larger the efficiency of the system, hence gates with large buoyancy (large eigenfrequency ω) are more efficient than heavier gates with large inertia. Moreover, figure 3(*a*) reveals that the capture factor can be larger than 0.5. This latter value corresponds to the maximum of a two-dimensional wave absorber working in synchronous resonance conditions with PTO coefficient equal to the radiation damping (Mei *et al.* 2005). Hence, nonlinear resonance has a significant beneficial effect on power extraction.

We now examine the behaviour of the bandwidth of instability expressed by (4.62) on the eigenfrequency ω for the optimal values of ν_{pto} (see figure 4). For large values of the inertia, i.e. small eigenfrequencies ω, the frequency band of instability approaches zero. Hence heavier gates are more difficult to resonate. Conversely, gates characterized by large values of the buoyancy can be easily resonated because the bandwidth of instability tends to increase. In summary, from a nonlinear point of view maximization of the performance of an array of OWCSs can be reached by choosing gates with large hydrodynamic stiffness.

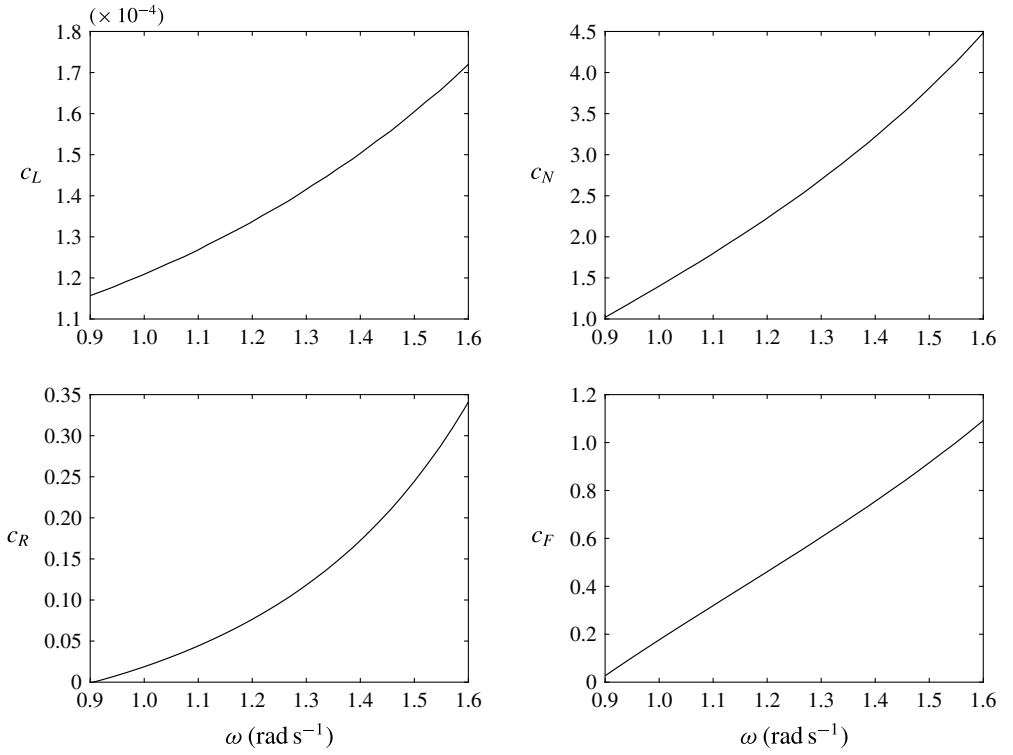

FIGURE 2. Behaviour of the coefficients of the evolution equation versus the eigenfrequency ω.

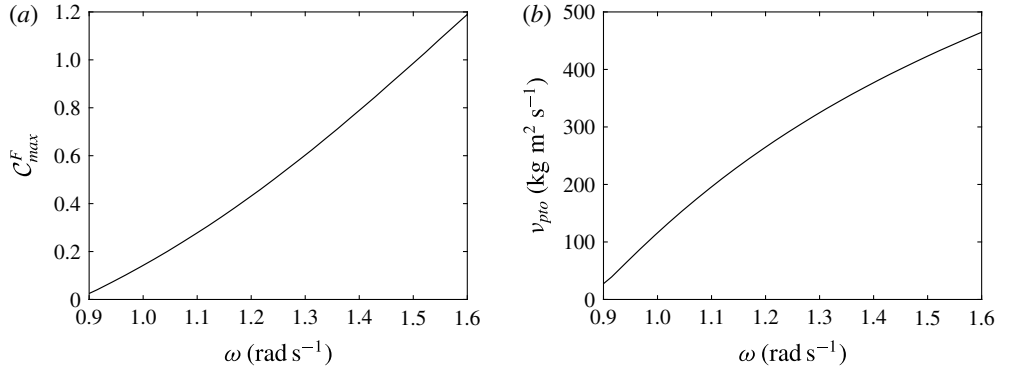

FIGURE 3. (*a*) Maximum of the capture factor $\mathcal{C}^F_{max}$ versus the eigenfrequency of the array ω. The capture factor reaches values larger than 0.5, i.e. the maximum that can be reached with synchronous motion only. (*b*) The optimal value of ν_{pto} versus eigenfrequency ω. The power take-off increases with ω.

Let us fix the eigenfrequency $\omega = 1.5$ rad s^{-1}. The corresponding values of the coefficients of the evolution equation are (see also figure 2):

$$c_L = 1.6 \times 10^{-4}, \quad c_N = 3.81, \quad c_R = 0.24, \quad c_F = 0.91, \tag{4.83a–d}$$

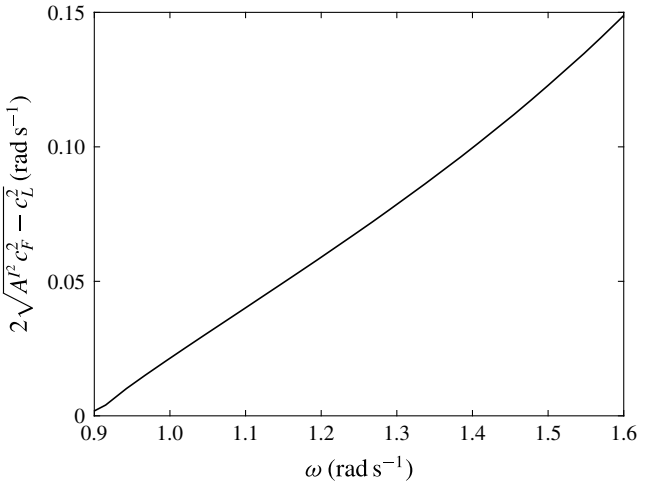

FIGURE 4. Bandwidth of instability versus the eigenfrequency of the array ω. Gates with small inertia I and large buoyancy C increase the eigenfrequency of the mode and render the subharmonic resonance more observable and efficient to extract power from water waves.

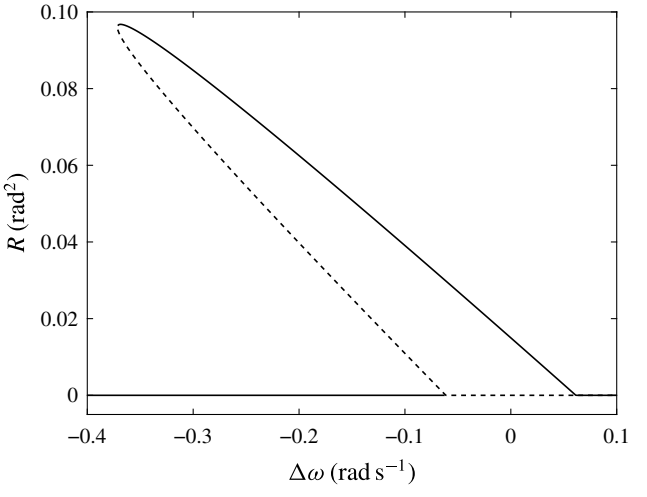

FIGURE 5. Bifurcation diagram of stable/unstable branches for the eigenfrequency of the natural mode $\omega = 1.5$ rad s^{-1}: – – –, unstable branch; ——, stable branch.

while the value of ν_{pto} is chosen following (4.69) (see figure 3*b*), i.e. $\nu_{pto} =$ 423 kg m^2 s^{-1}. Figure 5 shows the bifurcation diagram describing the dependence of the unstable and stable equilibria $R^{\pm}$ on $\Delta\omega$. The ellipse is inclined to the left hence the system behaves like a Duffing oscillator with soft spring. Similar behaviour has been already obtained for the subharmonic resonance of Venice gates analysed by Sammarco *et al.* (1997*a*,*b*).

Figure 6 shows the behaviour of the capture factor $\mathcal{C}^F$ given by (4.70) versus the detuning $\Delta\omega$. The maximum capture factor that can be reached is $\mathcal{C}^F \sim 1$ (see also

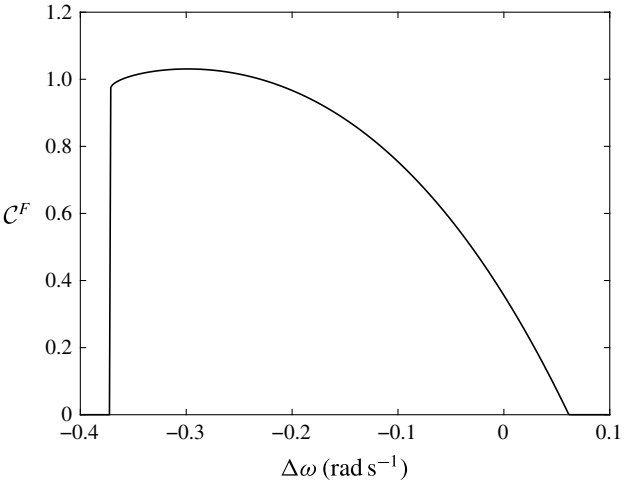

FIGURE 6. Behaviour of the capture factor $\mathcal{C}^F$ versus detuning $\Delta\omega$.

figure 3*a* for $\omega \sim 1.5$ rad s^{-1}), i.e. twice the size of the maximum possible for linear synchronous excitation in a channel (Mei *et al.* 2005).

4.7. *Results for modulated incident waves and* $Q = 2$

In this section we show the behaviour of the array in modulated incident waves with $\overline{A} = 0.1$ m. To investigate the effects of the gate stiffness on the minimum of the Melnikov function, consider the geometrical characteristics listed in table 3 and two different values of the eigenfrequency, that is, $\omega_1 = 1.5$ and $\omega_2 = 1.0$ rad s^{-1}. The respective values of the coefficients are

$$\left.\begin{array}{llll} c_{L1} = 1.6 \times 10^{-4}, & c_{N1} = 3.81, & c_{R1} = 0.24, & c_{F1} = 0.91, \\ c_{L2} = 1.2 \times 10^{-4}, & c_{N2} = 1.38, & c_{R2} = 0.02, & c_{F2} = 0.17. \end{array}\right\} \tag{4.84}$$

For each system we choose the PTO coefficient that satisfies (4.69) and maximizes power output. We obtain

$$\nu_1 = 423, \quad \nu_2 = 111 \text{ kg m}^2 \text{ s}^{-1}. \tag{4.85a,b}$$

Once the coefficients are evaluated, we assume $\Delta\omega = 0$ and derive the threshold for global chaos that can lead to homoclinic tangle. Figure 7 shows the dependence of the amplitude $\tilde{A}$ on the long-wave frequency Ω for both systems. The minimum value shifts to the right with increasing eigenfrequency of the array. Note that the bandwidth for gates with small buoyancy is narrower than that for gates characterized by small inertia. These results demonstrate that with respect to the case of heavier gates, systems with larger eigenfrequencies (more buoyant) can exhibit chaos for a broader range of long-wave forcing frequencies.

Now integrate system (4.74) numerically and investigate the occurrence of bifurcation scenarios with increasing amplitude $\tilde{A}$. Let us assume the eigenfrequency of the array to be $\omega = 1.5$ rad s^{-1} and fix the frequency of the long wave which corresponds to the minimum of the threshold shown in figure 7, i.e. $\Omega = 0.225$ rad s^{-1}.

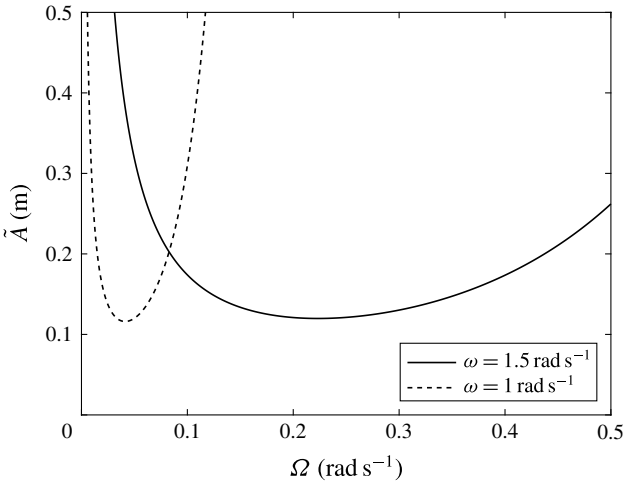

FIGURE 7. Melnikov criterion for determining lower bound of chaos in the plane $\tilde{A}$–Ω. Location of the minima depends on the eigenfrequency ω and tends to zero with the gate inertia. Moreover note that $\tilde{A} \to \infty$ for $\Omega \to (0, \infty)$ and chaotic response becomes impracticable.

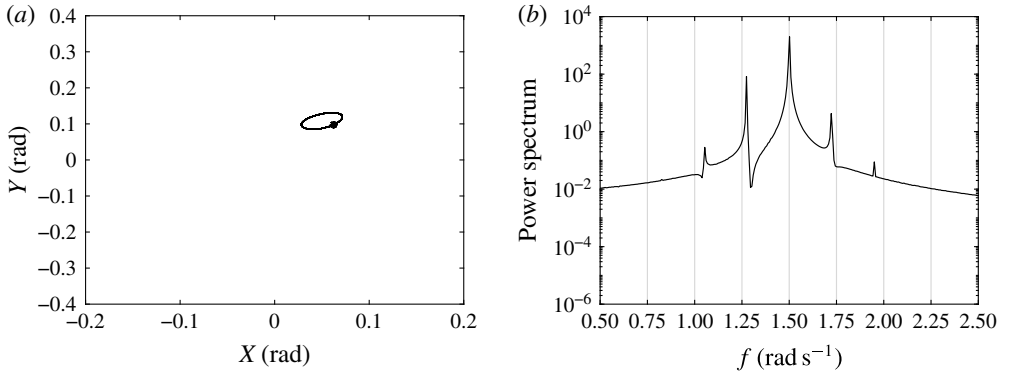

FIGURE 8. Gate array response at $\tilde{A} = 0.05$ m. Synchronous response. (*a*) Phase plane X–Y and Poincaré map for the evolution of $\overline{\theta}$; (*b*) power spectrum of the gate oscillation.

In order to follow bifurcation patterns we use the Poincaré map sampling time series of the gate envelope response $\overline{\theta}$ at times $t = 2\pi n/\Omega$, $n = 1, 2, 3 \ldots$, once transient motion disappears. To better analyse $\overline{\theta}$ we use the definition $\overline{\theta} = X + \mathrm{i}Y$ separating real and imaginary parts. Moreover, the output of (4.74) includes several harmonics, hence we further investigate the time series of the gate response $\Theta(t)$ looking at its power spectrum (Jordan & Smith 2011). For $\tilde{A} < 0.118$ m the response is synchronous and a stable $2\pi/\Omega$ periodic solution exists. Figure 8 shows the case for $\tilde{A} = 0.05$ m. The phase paths of the modal amplitude envelope together with its Poincaré map are shown in figure 8(*a*), while the power spectrum of the gate response is shown in figure 8(*b*). At $\tilde{A} = 0.118$ m a period doubling occurs and the response of the system becomes subharmonic. This case is shown in figure 9. A further increase of $\tilde{A}$ to

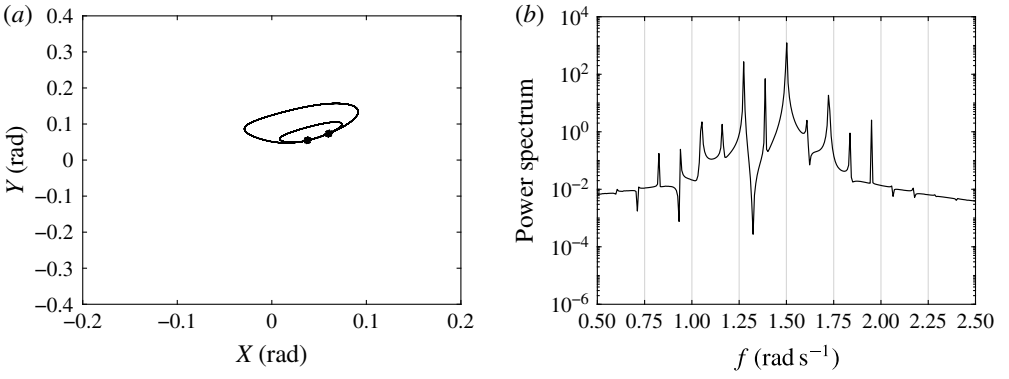

FIGURE 9. Subharmonic response at $\tilde{A} = 0.14$ m.

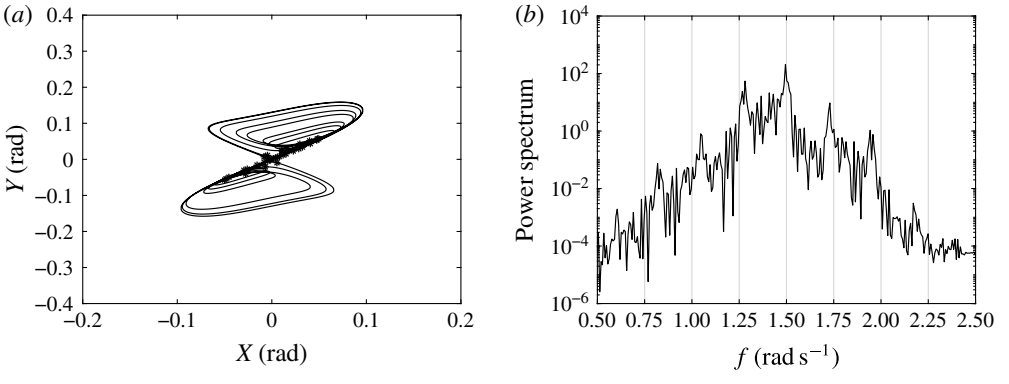

FIGURE 10. Chaos at $\tilde{A} = 0.2$ m.

values larger than $\tilde{A} = 0.151$ m reveals a stable period-four response, while chaos is fully developed for $0.158 < \tilde{A} < 0.173$ m. In the neighbourhood of $\tilde{A} = 0.173$ m a stable period-three response appears. For $\tilde{A} = 0.175$ m a chaotic regime reappears with a strange attractor of S shape, as shown in figure 10. This shape follows from the homoclinic path described by (4.79). The forcing term breaks the homoclinic connection and intersections between stable and unstable manifolds, causing chaos to occur. Moreover, the corresponding broad banded power spectrum (figure 10*b*) shows that a large number of frequencies is present. Note also the presence of peaks corresponding to the forcing frequency $\omega = 1.5$ rad s^{-1} and its subharmonics. Chaotic motion disappears again when the amplitude of the long wave is further increased up to values $\tilde{A} > 0.236$ m. Figure 11 shows subharmonic response with frequency downshift of the peak power spectrum for $\tilde{A} = 0.25$ m (Trulsen & Dysthe 1997). Indeed there is no peak located at $\omega = 1.5$ rad s^{-1}. Figure 12 shows the bifurcation diagram for the values of X at each time step. The same figure highlights period doubling routes to chaos, periodic windows (in this case around $\tilde{A} = 0.173$ m), chaotic bands and periodic responses with frequency downshift. Note also that values of $\tilde{A}$ corresponding to the bifurcation points almost satisfy the universal law found by

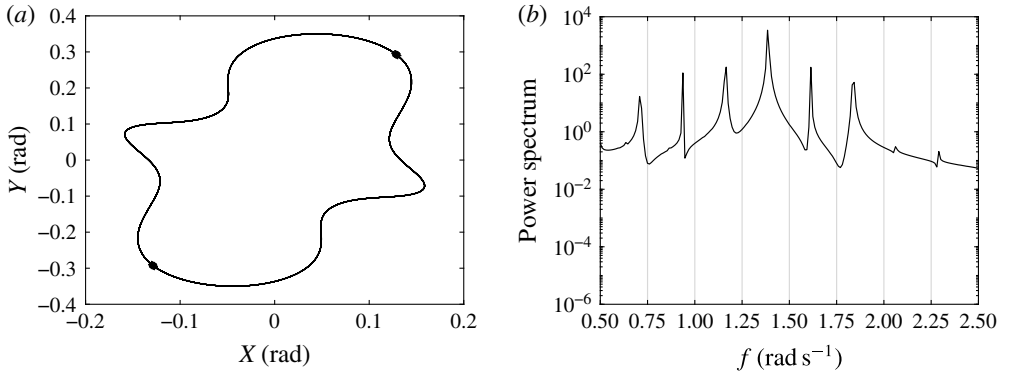

FIGURE 11. Period-two response and downshift at $\tilde{A} = 0.25$ m.

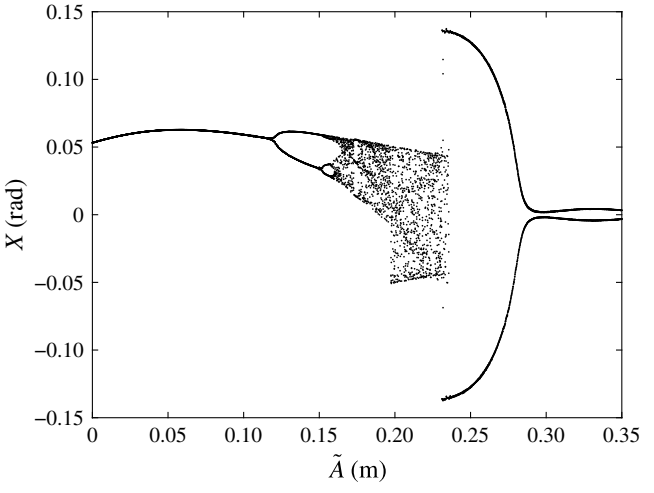

FIGURE 12. Period doubling scenarios as $\tilde{A}$ increases from 0 to 0.35 m.

Feigenbaum (Jordan & Smith 2011):

$$\lim_{n\to\infty} \frac{\tilde{A}_{n-1} - \tilde{A}_{n-2}}{\tilde{A}_n - \tilde{A}_{n-1}} = \delta = 4.669\ldots. \tag{4.86}$$

Recalling that the first bifurcation points are located at $\tilde{A}_1 = 0.118$, $\tilde{A}_2 = 0.151$ and $\tilde{A}_3 = 0.158$ (see also figure 12), we obtain

$$\frac{\tilde{A}_2 - \tilde{A}_1}{\tilde{A}_3 - \tilde{A}_2} = 4.7142\ldots \tag{4.87}$$

i.e. a value near the universal number δ found by Feigenbaum.

Finally we evaluate the effects of the chaotic response on the performance of the system. The incident wave amplitude is $\overline{A} + \tilde{A}\cos\Omega t$, hence the modulated incident

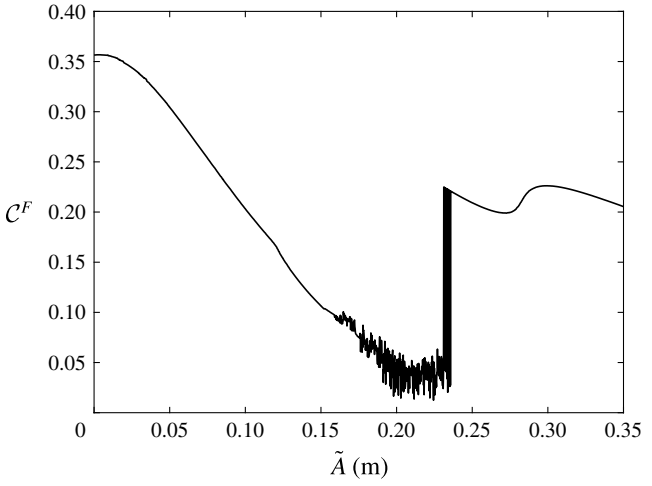

FIGURE 13. Behaviour of the capture factor of the array in modulated incident waves. Minima correspond to the range of $\tilde{A}$ where chaos occurs while the maximum is located at $\tilde{A} = 0$ m.

wave potential Φ_m^I is

$$\Phi_m^I = -\frac{\mathrm{i}g(\overline{A} + \tilde{A}\cos\Omega t)}{4\omega\cosh k_0 h}\cosh k_0(h+z)\mathrm{e}^{-\mathrm{i}(k_0 x + 2\omega t)} + *, \tag{4.88}$$

and the corresponding averaged energy influx

$$\lim_{\tau\to\infty} -\frac{\rho w}{\tau}\int_0^\tau\int_{-h}^0 \Phi_{m_t}^I \Phi_{m_x}^I \,\mathrm{d}z\,\mathrm{d}t = \frac{\gamma w\omega(2\overline{A}^2 + \tilde{A})}{4k_0}\left(1 + \frac{2k_0 h}{2\sinh 2k_0 h}\right). \tag{4.89}$$

The averaged generated power by the array can be evaluated numerically by solving the following integral:

$$P_m = \lim_{\tau\to\infty}\frac{1}{\tau}\int_0^\tau (\Theta_t)^2 \nu_{pto}\,\mathrm{d}t. \tag{4.90}$$

Figure 13 shows the capture factor of the array in modulated waves, defined as the ratio between P_m (4.90) and the energy influx (4.89) for the same range of $\tilde{A}$ used before. Note that the minimum of the efficiency of the system is located in the range of $\tilde{A}$ where chaos occurs, while the maximum corresponds to $\tilde{A} = 0$ m. When chaos disappears and regular motion returns with downshift, $\mathcal{C}^F$ spikes to $\sim$0.2 and starts again to decrease. In other words chaos and period doubling is detrimental in terms of wave energy extraction efficiency. We thus obtained a deterministic confirmation of the previous findings of Michele *et al.* (2016*a*,*b*) for gate energy production under stochastic incident wave spectra. Finally, note that the value of the capture factor for $\tilde{A} = 0$ m is $\mathcal{C}^F \sim 0.35$ and corresponds to the same value shown in figure 6 for $\omega =$ 3 rad s^{-1} and uniform incident waves.

5. Resonance of two trapped modes by one incident wave

Let us assume the scales (2.2) and the presence at the leading order $O(1)$ of two natural modes having different eigenfrequencies ω_1 and ω_2 with $\omega_2 > \omega_1$. Quadratic interactions at $O(\epsilon)$ generates four harmonics, i.e.

$$2\omega_1,\ 2\omega_2,\ (\omega_1+\omega_2),\ (\omega_2-\omega_1). \tag{5.1}$$

Let the incident wave have the frequency $(\omega_1+\omega_2)$, the multiple-scale expansion of the potentials, free-surface elevation and mode amplitude are assumed as follows:

$$\begin{aligned}\Phi^{\pm} &= \phi_{11}^{\pm}(x,y,z,t_2)\mathrm{e}^{-\mathrm{i}\omega_1 t}+\phi_{12}^{\pm}(x,y,z,t_2)\mathrm{e}^{-\mathrm{i}\omega_2 t}\\ &\quad+\epsilon\,[\phi_{21}^{\pm}(x,y,z,t_2)\mathrm{e}^{-2\mathrm{i}\omega_1 t}+\phi_{22}^{\pm}(x,y,z,t_2)\mathrm{e}^{-2\mathrm{i}\omega_2 t}+\phi_{23}^{\pm}(x,y,z,t_2)\mathrm{e}^{-\mathrm{i}(\omega_1+\omega_2)t}\\ &\quad+\phi_{24}^{\pm}(x,y,z,t_2)\mathrm{e}^{-\mathrm{i}(\omega_2-\omega_1)t}]+\epsilon^2[\phi_{31}^{\pm}(x,y,z,t_2)\mathrm{e}^{-\mathrm{i}\omega_1 t}+\phi_{32}^{\pm}(x,y,z,t_2)\mathrm{e}^{-\mathrm{i}\omega_2 t}]\\ &\quad+*+O(\epsilon^3),\end{aligned} \tag{5.2}$$

$$\begin{aligned}\zeta^{\pm} &= \zeta_{11}^{\pm}(x,y,t_2)\mathrm{e}^{-\mathrm{i}\omega_1 t}+\zeta_{12}^{\pm}(x,y,t_2)\mathrm{e}^{-\mathrm{i}\omega_2 t}\\ &\quad+\epsilon\,[\zeta_{21}^{\pm}(x,y,t_2)\mathrm{e}^{-2\mathrm{i}\omega_1 t}+\zeta_{22}^{\pm}(x,y,t_2)\mathrm{e}^{-2\mathrm{i}\omega_2 t}+\zeta_{23}^{\pm}(x,y,t_2)\mathrm{e}^{-\mathrm{i}(\omega_1+\omega_2)t}\\ &\quad+\zeta_{24}^{\pm}(x,y,t_2)\mathrm{e}^{-\mathrm{i}(\omega_2-\omega_1)t}]+\epsilon^2[\zeta_{31}^{\pm}(x,y,t_2)\mathrm{e}^{-\mathrm{i}\omega_1 t}+\zeta_{32}^{\pm}(x,y,t_2)\mathrm{e}^{-\mathrm{i}\omega_2 t}]\\ &\quad+*+O(\epsilon^3),\end{aligned} \tag{5.3}$$

$$\begin{aligned}\Theta^{\pm} &= \theta_{11}(y,t_2)\mathrm{e}^{-\mathrm{i}\omega_1 t}+\theta_{12}(y,t_2)\mathrm{e}^{-\mathrm{i}\omega_2 t}\\ &\quad+\epsilon\,[\theta_{21}(y,t_2)\mathrm{e}^{-2\mathrm{i}\omega_1 t}+\theta_{22}(y,t_2)\mathrm{e}^{-2\mathrm{i}\omega_2 t}+\theta_{23}(y,t_2)\mathrm{e}^{-\mathrm{i}(\omega_1+\omega_2)t}\\ &\quad+\theta_{24}(y,t_2)\mathrm{e}^{-\mathrm{i}(\omega_2-\omega_1)t}]+\epsilon^2[\theta_{31}(y,t_2)\mathrm{e}^{-\mathrm{i}\omega_1 t}+\theta_{32}(y,t_2)\mathrm{e}^{-\mathrm{i}\omega_2 t}]+*+O(\epsilon^3).\end{aligned} \tag{5.4}$$

5.1. *Leading-order problem* $O(1)$

This is the same problem already explained in § 4.1. The solution consists of trapped modes whose related potentials ϕ_{11}, ϕ_{12} have the form

$$\phi_{1j}^{\pm}=\mp\mathrm{i}\theta_j\sum_{q=1}^{Q}\sum_{m=1}^{\infty}\sum_{n=0}^{\infty}\frac{\omega_j b_{mqj}D_{nj}}{C_n\alpha_{mnj}}\mathrm{e}^{\mp\alpha_{mnj}x}\cos\frac{m\pi y}{b}\cosh k_{nj}(h+z)\equiv\mp\mathrm{i}\theta_j f_{1j}^{\pm}, \tag{5.5}$$

where the terms including the subscript $j=1,\,2$, are relative to the jth mode with eigenfrequency ω_j and modal form $\theta_{1j}=\{r_{1jq}\}\theta_j(t_2)$, $q=1,\ldots,Q$. To investigate the interactions between two modes it is necessary to consider the number of the gates $Q>2$ because the number of trapped modes is $Q-1$.

5.2. *The second-order problem* $O(\epsilon)$

As mentioned before, let us assume at $O(1)$ the existence of a couple of trapped modes N_1 and N_2 and the incident wave with frequency $(\omega_1+\omega_2)$. At the order $O(\epsilon)$ we have eight wave components generated by quadratic interactions of the $O(1)$ solution, i.e. the four harmonics (5.1) plus the respective complex conjugates.

We get the governing equation of each problem,

$$\nabla^2\phi_{2j}^{\pm}=0,\quad j=1,\ldots,4, \tag{5.6}$$

the relative boundary conditions on the moving gates,

$$\phi_{21_x}^{\pm}=\left[2\mathrm{i}\omega_1\theta_{21}(z+h_p)-\frac{\phi_{1_z}^{\pm}\theta_1}{\epsilon}\mp\mathrm{i}\omega_1 d\frac{\theta_1^2}{\epsilon}\right]H(z+h-c), \tag{5.7}$$

$$\phi^{\pm}_{22_x} = \left[2\mathrm{i}\omega_2\theta_{22}(z+h_p) - \frac{\phi^{\pm}_{2_z}\theta_2}{\epsilon} \mp \mathrm{i}\omega_2\, d\frac{\theta_2^2}{\epsilon}\right] H(z+h-c), \tag{5.8}$$

$$\phi^{\pm}_{23_x} = \left[\mathrm{i}(\omega_1+\omega_2)\theta_{23}(z+h_p) - \frac{\phi^{\pm}_{2_z}\theta_1 + \phi^{\pm}_{1_z}\theta_2}{\epsilon} \mp \mathrm{i}d(\omega_1+\omega_2)\frac{\theta_1\theta_2}{\epsilon}\right] H(z+h-c), \tag{5.9}$$

$$\phi^{\pm}_{24_x} = \left[\mathrm{i}(\omega_2-\omega_1)\theta_{24}(z+h_p) - \frac{\phi^{\pm}_{2_z}\theta_1^* + \phi^{\pm^*}_{1_z}\theta_2}{\epsilon} \mp \mathrm{i}d(\omega_2-\omega_1)\frac{\theta_1^*\theta_2}{\epsilon}\right] H(z+h-c), \quad x = x^{\pm}, \tag{5.10}$$

the mixed boundary conditions on the free surface,

$$\phi^{\pm}_{21_z} = \phi^{\pm}_{21}\frac{4\omega_1^2}{g}, \tag{5.11}$$

$$\phi^{\pm}_{22_z} = \phi^{\pm}_{22}\frac{4\omega_2^2}{g}, \tag{5.12}$$

$$\phi^{\pm}_{23_z} = \phi^{\pm}_{23}\frac{(\omega_1+\omega_2)^2}{g}, \tag{5.13}$$

$$\phi^{\pm}_{24_z} = \phi^{\pm}_{24}\frac{(\omega_2-\omega_1)^2}{g}, \quad z = 0, \tag{5.14}$$

and the corresponding free-surface elevations,

$$\eta^{\pm}_{21} = \frac{2\mathrm{i}\omega_1}{g}\phi^{\pm}_{21}, \tag{5.15}$$

$$\eta^{\pm}_{22} = \frac{2\mathrm{i}\omega_2}{g}\phi^{\pm}_{22}, \tag{5.16}$$

$$\eta^{\pm}_{23} = \frac{\mathrm{i}(\omega_1+\omega_2)}{g}\phi^{\pm}_{23}, \tag{5.17}$$

$$\eta^{\pm}_{24} = \frac{\mathrm{i}(\omega_2-\omega_1)}{g}\phi^{\pm}_{24}, \quad z = 0. \tag{5.18}$$

As in § 4.2, we obtain the second-order solution of each jth wave field component,

$$\phi^{\pm}_{2j} = \tilde{\theta}_j \sum_{p=0}^{\infty}\sum_{l=0}^{\infty} \frac{\Delta_{plj}}{\alpha_{plj}\epsilon} \mathrm{e}^{\pm\mathrm{i}\alpha_{plj}x} \cos\frac{p\pi y}{b} \cosh k_{lj}(h+z), \quad j = 1, \ldots, 4, \tag{5.19}$$

where $\tilde{\theta}(t) = \{\theta_1^2,\ \theta_2^2,\ \theta_1\theta_2,\ \theta_1\theta_2^*\}$ is the vector that contains the combinations of the resonated mode amplitudes, k_{lj} are the roots of the dispersion relations,

$$\left.\begin{array}{cc} 4\omega_1^2 = gk_{01}\tanh k_{01}h, & 4\omega_1^2 = -g\bar{k}_{l1}\tan\bar{k}_{l1}h, \\ 4\omega_2^2 = gk_{02}\tanh k_{02}h, & 4\omega_2^2 = -g\bar{k}_{l2}\tan\bar{k}_{l2}h, \\ (\omega_1+\omega_2)^2 = gk_{03}\tanh k_{03}h, & (\omega_1+\omega_2)^2 = -g\bar{k}_{l3}\tan\bar{k}_{l3}h, \\ (\omega_2-\omega_1)^2 = gk_{04}\tanh k_{04}h, & (\omega_2-\omega_1)^2 = -g\bar{k}_{l4}\tan\bar{k}_{l4}h, \\ k_{lj} = \mathrm{i}\bar{\kappa}_l, \quad j = 1, \ldots, 4, & l = 1, \ldots, \infty, \end{array}\right\} \tag{5.20}$$

while Δ_{plj} is a complex coefficient evaluated in appendix A. Similarly to the previous case, the gate motion at this order is null ($\theta_{2j} = 0$, $j = 1, \ldots, 4$), however there are propagating waves that radiate energy to infinity and damp mode motion through cubic interactions at the third order.

5.3. *The coupled evolution equations*

At this order we apply the solvability condition which is found by Green's formula:

$$0 = \frac{\omega_j^2}{g}\int_0^b \mathrm{d}y \left(\int_{-\infty}^0 f_{1j}^- \mathcal{F}_{3j}^- \,\mathrm{d}x - \int_0^\infty f_{1j}^+ \mathcal{F}_{3j}^+ \,\mathrm{d}x\right) + 2\int_0^b \mathrm{d}y \int_{-h}^0 \overline{f_j \mathcal{G}_{3j}}\,\mathrm{d}z + \sum_{q=1}^{Q}\left(\frac{\mathrm{i}\mathcal{D}_{3j} r_{1jq}}{\rho} - \frac{\nu_{pto} r_{1jq}^2 \omega_j \theta_j}{\rho \epsilon^2}\right), \quad j = 1, 2. \tag{5.21}$$

Details of the forcing terms in the latter equation can be found in appendix B. Carrying out the integrals of (5.21) and grouping the terms according to θ_{11}, θ_{12}, $\theta_{11}\,|\theta_{11}|^2$, $\theta_{11}\,|\theta_{12}|^2$, $\theta_{12}\,|\theta_{12}|^2$, $\theta_{12}\,|\theta_{11}|^2$, θ_{11}^*, θ_{12}^*, we obtain two coupled evolution equations for both modal oscillations θ_{11} and θ_{12}:

$$-\mathrm{i}\theta_{11_t} = \theta_{11}|\theta_{11}|^2(c_N + \mathrm{i}c_R) + \theta_{11}|\theta_{12}|^2(c_S + \mathrm{i}c_U) + A\theta_{12}^* c_F + \mathrm{i}\theta_{11}\nu_{pto} c_L, \tag{5.22}$$

$$-\mathrm{i}\theta_{12_t} = \theta_{12}|\theta_{12}|^2(d_N + \mathrm{i}d_R) + \theta_{12}|\theta_{11}|^2(d_S + \mathrm{i}d_U) + A\theta_{11}^* d_F + \mathrm{i}\theta_{12}\nu_{pto} d_L, \tag{5.23}$$

where the coupling coefficients are evaluated in a similar manner as explained in § 4.3. Differently to the case of single-mode subharmonic excitation we have two new pairs of coefficients as in the edge wave theories, c_S, d_S, c_U, d_U, that represent the coupling between the modes. Note also that in (5.22) the incident wave amplitude A is multiplied by the complex conjugate of θ_{12}, while in (5.23) the same term is multiplied by θ_{11}^*. This depends on the fact that the incident wave frequency is assumed to be equal to $(\omega_1 + \omega_2)$ and not equal to twice the eigenfrequency of a single mode. Now consider the detuning of the incident wave frequency $\Delta\omega$ with $\Delta\omega/\omega \sim O(\epsilon^2)$ and let us assume the following change of variables:

$$\theta_j = \overline{\theta}_j \mathrm{e}^{-\mathrm{i}\Delta\omega_j t}, \quad j = 1, 2, \tag{5.24}$$

where $\Delta\omega = \Delta\omega_1 + \Delta\omega_2$. Then the evolution equations modify as follows:

$$-\mathrm{i}\overline{\theta}_{11_t} = \Delta\omega_1\overline{\theta}_{11} + \overline{\theta}_{11}|\overline{\theta}_{11}|^2(c_N + \mathrm{i}c_R) + \overline{\theta}_{11}|\overline{\theta}_{12}|^2(c_S + \mathrm{i}c_U) + A\overline{\theta}_{12}^* c_F + \mathrm{i}\overline{\theta}_{11}\nu_{pto} c_L, \tag{5.25}$$

$$-\mathrm{i}\overline{\theta}_{12_t} = \Delta\omega_2\overline{\theta}_{12} + \overline{\theta}_{12}|\overline{\theta}_{12}|^2(d_N + \mathrm{i}d_R) + \overline{\theta}_{12}|\overline{\theta}_{11}|^2(d_S + \mathrm{i}d_U) + A\overline{\theta}_{11}^* d_F + \mathrm{i}\overline{\theta}_{12}\nu_{pto} d_L. \tag{5.26}$$

5.4. *Analysis of the coupled equations and theoretical results*

Consider an array of $Q = 4$ gates with characteristics listed in table 3. We obtain two odd natural modes and a single even mode (see also Sammarco *et al.* 2013). Interaction between odd–even modes yields the coefficients c_F, d_F equal to zero and the system of (5.25)–(5.26) becomes unforced. As a consequence, we can consider

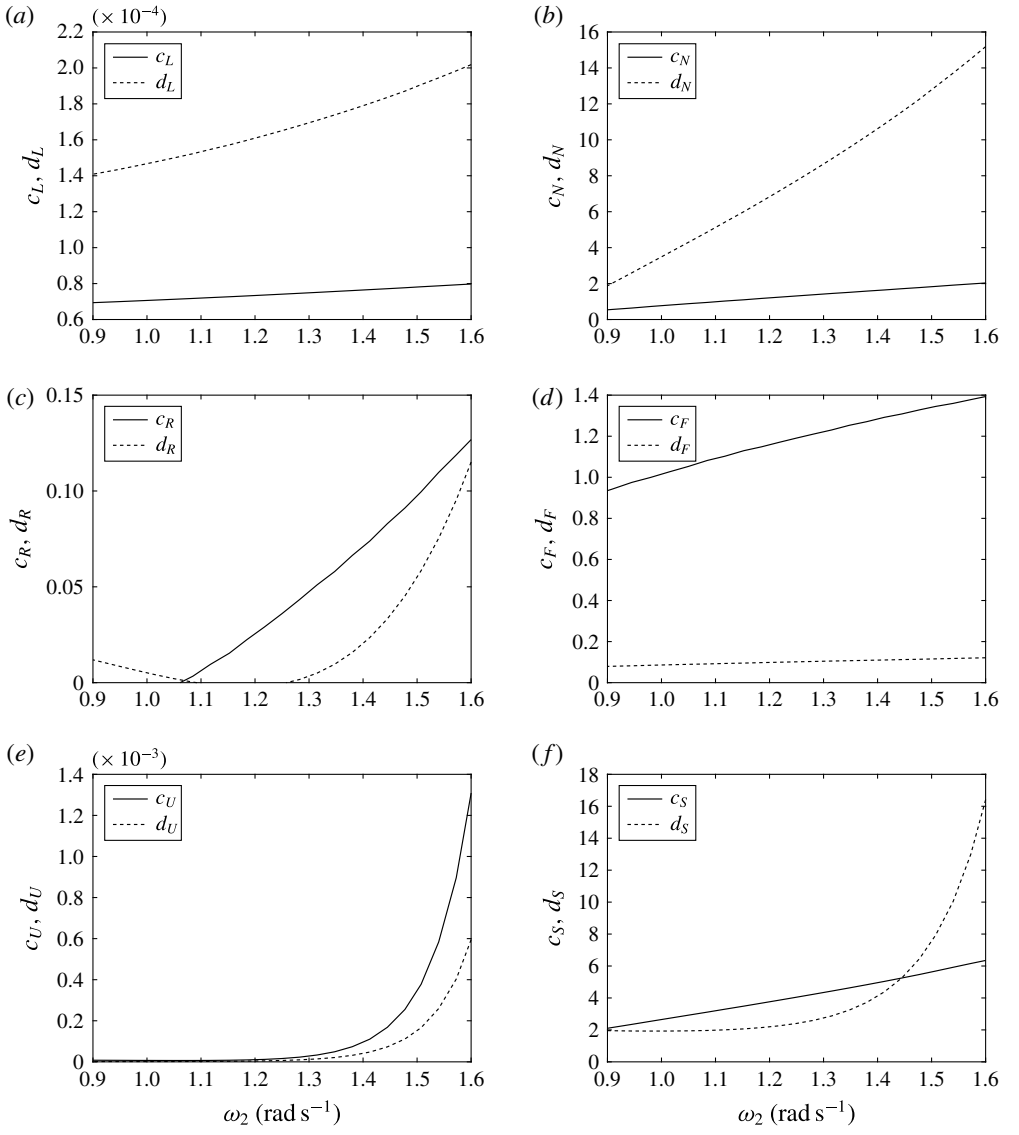

FIGURE 14. Behaviour of the coefficients of the evolution equations versus the eigenfrequency of the mode N_2, ω_2.

the interaction between the odd modes only, with shape $r_{11q} = \{1, 0.41, -0.41, -1\}$ and $r_{12q} = \{1, -2.41, 2.41, -1\}$. Sample values of the coefficients of (5.25)–(5.26) are shown in figure 14. Note that c_U and d_U (figure 14*e*) are very small if compared to the others and tend to increase for large eigenfrequencies while c_F is larger than d_F although $\omega_1 < \omega_2$ for fixed gate characteristics. This has an important consequence because N_1 can be forced more easily by the incident waves.

Now define $\overline{\theta}_{1j}$ in action-angle variables form, i.e. $\overline{\theta}_{1j} = \mathrm{i}\sqrt{R_j}\mathrm{e}^{\mathrm{i}\psi_j}$, and neglect c_U, d_U with respect to the other coefficients to reduce the algebra without simplifying the physics. Then, from (5.25)–(5.26), we obtain a system of four real differential

equations:

$$\left.\begin{aligned} R_{1_t} &= -2R_1\left[R_1 c_R + A c_F\sqrt{\frac{R_2}{R_1}}\sin\psi + \nu_{pto} c_L\right] \\ R_{2_t} &= -2R_2\left[R_2 d_R + A d_F\sqrt{\frac{R_1}{R_2}}\sin\psi + \nu_{pto} d_L\right] \\ \psi_{1_t} &= \Delta\omega_1 - A c_F\sqrt{\frac{R_2}{R_1}}\cos\psi + R_1 c_N + R_2 c_S \\ \psi_{2_t} &= \Delta\omega_2 - A d_F\sqrt{\frac{R_1}{R_2}}\cos\psi + R_1 d_S + R_2 d_N, \end{aligned}\right\} \tag{5.27}$$

in which $\psi = \psi_1 + \psi_2$ denotes the sum of the modal phases. After a long time the system reaches equilibrium, hence we now focus our attention on determining the fixed points of (5.27). The trivial fixed point is at

$$R_1 = R_2 = 0, \quad \psi^* = \cos^{-1}\frac{\Delta\omega}{A(c_F + d_F)}, \tag{5.28a,b}$$

while non-trivial fixed points related to unstable and stable equilibria correspond to the roots of the system

$$R_2 = \frac{1}{2d_R}\left[-\nu_{pto} d_L + \sqrt{\nu_{pto}^2 d_L^2 + \frac{4 d_F d_R R_1(\nu_{pto} c_L + c_R R_1)}{c_F}}\right], \tag{5.29}$$

$$\begin{aligned} &[\Delta\omega + R_1(c_N + d_S) + R_2(d_N + c_S)]^2 + (R_1 c_R + \nu_{pto} c_L + R_2 d_R + \nu_{pto} d_L)^2 \\ &- A^2\left(\sqrt{\frac{R_2}{R_1}} c_F + \sqrt{\frac{R_1}{R_2}} d_F\right)^2 = 0, \end{aligned} \tag{5.30}$$

which can be found numerically. Note that if $R_1 = 0$ also $R_2 = 0$ and triad resonance does not occur. Stability analysis of the linearized system (5.25)–(5.26) at the origin allows us to find the threshold of resonance triad,

$$A > \nu_{pto}\sqrt{\frac{c_L d_L}{c_F d_F}}, \tag{5.31}$$

hence the amplitude of the incident wave must be larger than the latter quantity to trigger mode–mode interactions. Once the equilibrium states R_1 and R_2 are evaluated we determine the sum of the modal phases by manipulating ψ_{1_t} and ψ_{2_t}:

$$\psi^0 = \cos^{-1}\left[\frac{\Delta\omega + R_1(c_N + d_S) + R_2(c_S + d_N)}{A\left(c_F\sqrt{\frac{R_2}{R_1}} + d_F\sqrt{\frac{R_1}{R_2}}\right)}\right]. \tag{5.32}$$

Substitution of $\psi = \psi^0$ inside (5.27) gives $\Delta\omega_1$ and $\Delta\omega_2$. Physically, the latter terms are the speed along the limit cycles in the complex plane $\mathrm{Re}\{\theta\}, \mathrm{Im}\{\theta\}$. The generated

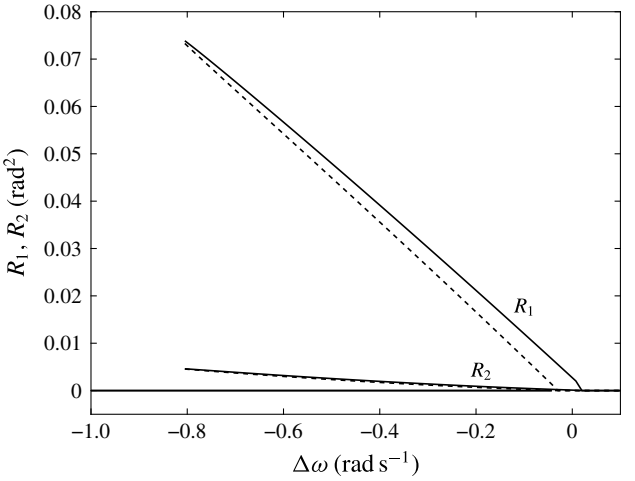

FIGURE 15. Equilibrium branches of R_1 ad R_2 versus detuning of the incident wave $\Delta\omega$. The solid lines represent the stable equilibrium branch while the dotted lines represent the unstable branch.

power due to triad resonance is finally given by

$$\begin{aligned} P_t &= \lim_{\tau\to\infty}\frac{1}{\tau}\int_0^\tau [(\theta_{11}\mathrm{e}^{-\mathrm{i}(\omega_1+\Delta\omega_1)t}+\theta_{12}\mathrm{e}^{-\mathrm{i}(\omega_2+\Delta\omega_2)t}+*)_t]^2\nu_{pto} \\ &= 2\nu_{pto}\left[(\Delta\omega_1+\omega_1)^2\sum_{q=1}^{Q} r_{11q}^2 R_1^0+(\Delta\omega_2+\omega_2)^2\sum_{q=1}^{Q} r_{12q}^2 R_2^0\right]. \end{aligned} \tag{5.33}$$

Now focus the attention on a fixed OWSC configuration and analyse the effects of triad resonance on the performances of the array. Let us consider the case where the system has the eigenfrequency $\omega_2 = 1.5$ rad s^{-1}. Solution of the eigenvalue condition at the first order gives the eigenfrequency of the mode N_1, i.e. $\omega_1 = 0.9$ rad s^{-1}. The corresponding evolution equation coefficients are (see also figure 14):

$$\left.\begin{array}{llll} c_N = 1.84, & c_R = 0.1, & c_F = 1.34, & c_S = 5.68, \\ d_N = 12.96, & d_R = 0.06, & d_F = 0.11, & d_S = 7.93. \end{array}\right\} \tag{5.34}$$

Choose the ν_{pto} which maximizes power output for perfect resonance, i.e. $\Delta\omega_1 = \Delta\omega_2 = 0$ and $A = 0.05$ m. Maximization of (5.33) yields $\nu_{pto} = 120$ kg m^2 s^{-1}. The corresponding equilibrium branches of R_1 and R_2 are plotted in figure 15. Simple numerical evaluation of the eigenvalues reveals results similar to the case of single-mode resonance. The continuous lines correspond to stable fixed points, while the dot lines are related to unstable saddles.

At this point, we evaluate the efficiency of the system excited through mode-mode interactions. Figure 16 shows the behaviour of $\mathcal{C}^F$ versus the frequency of the incident waves. The maximum of the capture factor is ∼0.25, hence the effect of triad interaction is not as significant as the subharmonic case (see figure 6) but positive anyway.

6. Conclusions

We have investigated theoretically the nonlinear effects on the performance of an array of oscillating wave surge converters in a channel. We extended the theory of

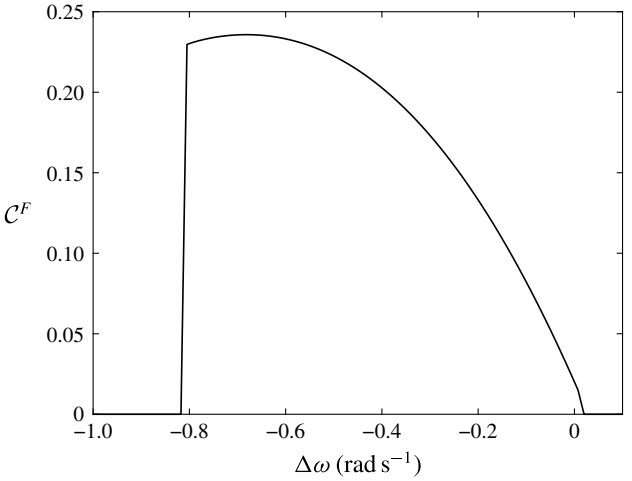

FIGURE 16. Behaviour of the capture factor due to triad resonance. Mode–mode interaction yields smaller values of $\mathcal{C}^F$ than the subharmonic resonance of a single mode.

Sammarco *et al.* (1997*a*,*b*) using scales which simplified considerably the required algebra for the coefficients of the Stuart–Landau evolution equation. This is because unlike the Venice gates, the OWSCs considered here do not span the entire water depth but are placed upon a vertical fixed wall on a rigid bottom. The dependence of the coefficients on the eigenfrequency of the system has been examined. We have derived a formula to evaluate the maximum capture factor in uniform incident waves and found that subharmonic excitation yields very large values of the capture factor. Moreover we showed that the array with large eigenfrequency induces an increase in the efficiency, hence heavier gates should be avoided in order to maximize energy production in nonlinear regimes. The dependence of the evolution equation coefficients on the eigenfrequency of the system has allowed us to determine thresholds of instability, equilibrium points of the dynamical system and the optimal values of the PTO coefficients which maximize power output. We have shown that gates with large buoyancy yield the array susceptible to subharmonic resonance, conversely, heavier gates are difficult to resonate. Detailed analysis was performed to see the effects of modulated incident waves on the dynamics of the array. We found thresholds above which homoclinic tangles and so chaotic regimes occur. We have shown that arrays with large eigenfrequency can exhibit chaos for a broader range of long-wave forcing frequencies. Numerical investigation of the non-autonomous dynamical system has allowed us to find bifurcation scenarios. By increasing the amplitude of the incident wave envelope we have reproduced period doubling cascades, chaotic bands and periodic windows. We have found that chaos disappears for large values of the periodic modulation. The response of the array is then subharmonic with the gate envelope and a frequency downshift of the peak power spectrum occurs. The efficiency of the system decreases significantly when period doubling and chaotic regimes occur. Finally we analysed the case of mode–mode interactions. We have found that effects of triad interactions on the generated power are not as significant than the pure subharmonic case, yet relevant. However this final investigation could be important for a fuller understanding of OWSCs complicated dynamics and to facilitate interpretation of experimental data results. We have assumed that the torque exerted by the ideal PTO increases linearly with the angular velocity of the gate.

We have obtained that nonlinear resonance is possible for PTO coefficient values at $O(\epsilon^2)$. Several mechanisms not considered here such as friction losses, viscous damping and nonlinear PTO laws clearly influence the gate dynamics. However, to analyse these higher-order effects it is necessary also to study in detail the mechanics of a specific generator. This subject will be investigated soon. A second theoretical question remains, i.e. the analysis of the subharmonic resonance in open sea where natural modes of a finite array of OWSCs are nearly trapped and radiate energy. These questions represent a fairly open and challenging research subject and will be addressed in the near future to better understand the dynamics of such devices.

Acknowledgements

This research was partially funded by 'Sales SpA'. The authors would like to mention that without Professor C. C. Mei's virtual supervision, none of this research would have been possible. Fruitful discussions with Dr E. Renzi are kindly acknowledged.

Appendix A. Details of the coefficient Δ_{pln}

Following the same steps for the second-order solution of § 4.2 we obtain

$$\Delta_{pl1} = \frac{1}{2\delta_p C_{l1}} \sum_{q=1}^{Q} \sum_{m=1}^{\infty} \sum_{n=0}^{\infty} \left\{ \frac{\omega_1 b_{(m+p)q1} b_{mq1} D_{n1} C_{ln11}}{C_{n1}} \left(\frac{1}{\alpha_{mn1}} + \frac{1}{\alpha_{(m+p)n1}} \right) - d\omega_1 E_{l1} b_{(m+p)q1} b_{mq1} \right\}, \tag{A 1}$$

$$\Delta_{pl2} = \frac{1}{2\delta_p C_{l2}} \sum_{q=1}^{Q} \sum_{m=1}^{\infty} \sum_{n=0}^{\infty} \left\{ \frac{\omega_2 b_{(m+p)q2} b_{mq2} D_{n2} C_{ln22}}{C_{n2}} \left(\frac{1}{\alpha_{mn2}} + \frac{1}{\alpha_{(m+p)n2}} \right) - d\omega_2 E_{l2} b_{(m+p)q1} b_{mq1} \right\}, \tag{A 2}$$

$$\begin{aligned} \Delta_{pl3} = \frac{1}{2\delta_p C_{l3}} \sum_{q=1}^{Q} \sum_{m=1}^{\infty} \sum_{n=0}^{\infty} \Bigg\{ & b_{(m+p)q1} \frac{\omega_2 b_{mq2} D_{n2} C_{ln32}}{C_{n2} \alpha_{mn2}} + b_{mq1} \frac{\omega_2 b_{(m+p)q2} D_{n2} C_{ln32}}{C_{n2} \alpha_{(m+p)n2}} \\ & + b_{(m+p)q2} \frac{\omega_1 b_{mq1} D_{n1} C_{ln31}}{C_{n1} \alpha_{mn1}} + b_{mq2} \frac{\omega_1 b_{(m+p)q1} D_{n1} C_{ln31}}{C_{n1} \alpha_{(m+p)n1}} \\ & - d\omega_1 E_{l3} (\omega_2 + \omega_1) (b_{(m+p)q1} b_{mq2} + b_{mq1} b_{(m+p)q2} + b_{(m+p)q2} b_{mq1} + b_{mq2} b_{(m+p)q1}) \Bigg\}, \end{aligned} \tag{A 3}$$

$$\begin{aligned} \Delta_{pl4} = \frac{1}{2\delta_p C_{l4}} \sum_{q=1}^{Q} \sum_{m=1}^{\infty} \sum_{n=0}^{\infty} \Bigg\{ & b_{(m+p)q1} \frac{\omega_2 b_{mq2} D_{n2} C_{ln42}}{C_{n2} \alpha_{mn2}} + b_{mq1} \frac{\omega_2 b_{(m+p)q2} D_{n2} C_{ln42}}{C_{n2} \alpha_{(m+p)n2}} \\ & - b_{(m+p)q2} \frac{\omega_1 b_{mq1} D_{n1} C_{ln41}}{C_{n1} \alpha_{mn1}} - b_{mq2} \frac{\omega_1 b_{(m+p)q1} D_{n1} C_{ln41}}{C_{n1} \alpha_{(m+p)n1}} \\ & - d\omega_1 E_{l4} (\omega_2 - \omega_1) (b_{(m+p)q1} b_{mq2} + b_{mq1} b_{(m+p)q2} + b_{(m+p)q2} b_{mq1} + b_{mq2} b_{(m+p)q1}) \Bigg\}, \end{aligned} \tag{A 4}$$

where the coefficients C_{ln1} and C_{ln2} have the same form as (4.33), while

$$C_{ln31} = \frac{1}{k_{l3}^2 - k_{n1}^2}\left[\cosh k_{n1}h \cosh k_{l3}h \left(\frac{(\omega_1+\omega_2)^2}{g^2} - k_{n1}^2\right) + k_{n1}^2 \cosh k_{n1}c \cosh k_{l3}c - k_{l3}k_{n1} \sinh k_{n1}h \sinh k_{l3}h\right], \tag{A 5}$$

$$C_{ln32} = \frac{1}{k_{l3}^2 - k_{n2}^2}\left[\cosh k_{n2}h \cosh k_{l3}h \left(\frac{(\omega_1+\omega_2)^2}{g^2} - k_{n2}^2\right) + k_{n2}^2 \cosh k_{n2}c \cosh k_{l3}c - k_{l3}k_{n2} \sinh k_{n2}h \sinh k_{l3}h\right], \tag{A 6}$$

$$C_{ln41} = \frac{1}{k_{l4}^2 - k_{n1}^2}\left[\cosh k_{n1}h \cosh k_{l4}h \left(\frac{(\omega_2-\omega_1)^2}{g^2} - k_{n1}^2\right) + k_{n1}^2 \cosh k_{n1}c \cosh k_{l3}c - k_{l4}k_{n1} \sinh k_{n1}h \sinh k_{l4}h\right], \tag{A 7}$$

$$C_{ln42} = \frac{1}{k_{l4}^2 - k_{n2}^2}\left[\cosh k_{n2}h \cosh k_{l4}h \left(\frac{(\omega_2-\omega_1)^2}{g^2} - k_{n2}^2\right) + k_{n2}^2 \cosh k_{n2}c \cosh k_{l4}c - k_{l4}k_{n2} \sinh k_{n2}h \sinh k_{l4}h\right], \tag{A 8}$$

$$E_{lj} = \frac{1}{k_{lj}}(\sinh k_{lj}h - \sinh k_{lj}c), \quad j = 1, \ldots, 4. \tag{A 9}$$

Appendix B. Details of the forcing terms for the solvability condition (5.21)

Recall the solvability condition for each jth harmonic:

$$\frac{\omega_j^2}{g}\int_0^b \mathrm{d}y \left(\int_{-\infty}^0 f_{1j}^- \mathcal{F}_{3j}^- \,\mathrm{d}x - \int_0^\infty f_{1j}^+ \mathcal{F}_{3j}^+ \,\mathrm{d}x\right) + 2\int_0^b \mathrm{d}y \int_{-h}^0 \overline{f_j \mathcal{G}_{3j}}\,\mathrm{d}z + \sum_{q=1}^{Q}\left(\frac{\mathrm{i}\mathcal{D}_{3j} r_{1jq}}{\rho} - \frac{\nu_{pto} r_{1jq}^2 \omega_j \theta_j}{\rho \epsilon^2}\right) = 0, \quad j = 1, 2. \tag{B 1}$$

The forcing term for the free-surface mixed condition is defined as

$$\mathcal{F}_{3j}^{\pm} = \pm \frac{2 f_{1j}^{\pm} \theta_{t_j}}{\omega_j}, \quad j = 1, 2, \tag{B 2}$$

the forcing terms for the kinematic condition on the gates are respectively

$$\begin{aligned}\mathcal{G}_{31}^{\pm} = &-\{[\theta_{11}|\theta_{12}|^2(\mathrm{i} r_{12q} f_{23_z}^{\pm} - \mathrm{i} r_{12q} f_{24_z}^{\pm *}) + \theta_{11}|\theta_{11}|^2 \mathrm{i} f_{11_z} r_{11q}] \\ &- A\theta_{12}^*(\phi_z^{\pm A} r_{12q}) - r_{11q}\theta_{11_t}(z + h_p) \pm 2\theta_{11}|\theta_{11}|^2 \, d\omega_1 f_{21} r_{11p} \\ &\pm \theta_{11}|\theta_{12}|^2 \, d(\omega_1 + \omega_2) f_{23} r_{12q} \\ &\pm \theta_{11}|\theta_{12}|^2 \, d(\omega_2 - \omega_1) f_{24}^* r_{12q}\} \, H(z + h - c),\end{aligned} \tag{B 3}$$

and

$$\begin{aligned}\mathcal{G}_{32}^{\pm} = & -\{[\theta_{12}|\theta_{11}|^2(\mathrm{i}r_{11q}f_{23_z}^{\pm}+\mathrm{i}r_{11q}f_{24_z}^{\pm})+\theta_{12}|\theta_{12}|^2\mathrm{i}f_{12_z}r_{12q}]\\ & -A\theta_{11}^*(\phi_z^{\pm A}r_{11q})-r_{12q}\theta_{12_t}(z+h_p)\pm 2\theta_{12}|\theta_{12}|^2\,d\omega_2 f_{22}r_{12p}\\ & \pm\theta_{12}|\theta_{11}|^2\,d(\omega_1+\omega_2)f_{23}r_{11p}\\ & \pm\theta_{12}|\theta_{11}|^2\,d(\omega_2-\omega_1)f_{24}r_{11p}\}\,H(z+h-c),\end{aligned} \tag{B 4}$$

while the remaining forcing terms for the equation of motion of both modal oscillations are given by

$$\begin{aligned}\mathcal{D}_{31}^{\pm} = & -\rho\int_{(q-1)a}^{qa}\mathrm{d}y\left\{\int_{-h_p}^{0}\mathrm{d}z\,[-6f_{11}r_{11q}^2\theta_{11}|\theta_{11}|^2\omega_1-6f_{12}r_{12q}r_{11q}\theta_{11}|\theta_{12}|^2\omega_2\right.\\ & -4f_{11}r_{12q}^2\theta_{11}|\theta_{12}|^2\omega_1-2\mathrm{i}f_{11}\theta_{11_t}](z+h_p)+\frac{f_{11}^3\omega_1^3}{g^2}\theta_{11}|\theta_{11}|^2+\frac{f_{12}^2f_{11}\omega_1\omega_2^2}{g^2}\theta_{11}|\theta_{12}|^2\\ & +2h_p\Delta\left[\frac{f_{12}\omega_2}{g}f_{24}^*(\omega_2-\omega_1)\theta_{11}|\theta_{12}|^2+\frac{f_{12}\omega_2}{g}f_{23}(\omega_2+\omega_1)\theta_{11}|\theta_{12}|^2\right.\\ & \left.+\ 2\frac{f_{11}\omega_1}{g}f_{21}\omega_1\theta_{11}|\theta_{11}|^2\right]-Ah_p(\omega_1+\omega_2)\Delta\left(\pm\frac{f_{12}\omega_2}{g}\phi^{\pm A}\theta_{12}^*\right)\Bigg\}+2\omega_1Ir_{11q}\mathrm{i}\theta_{11_t}\\ & +2\rho\,d\int_{(q-1)a}^{qa}\mathrm{d}y\int_{-h_p}^{0}\mathrm{d}z\,(\theta_{11}|\theta_{11}|^2 2\omega_1f_{21}r_{11q}+\theta_{11}|\theta_{12}|^2(\omega_1+\omega_2)f_{23}r_{12q}\\ & +\theta_{11}|\theta_{12}|^2(\omega_2-\omega_1)f_{24}^*r_{12q})+\rho\,d\int_{(q-1)a}^{qa}\mathrm{d}y\left[\theta_{11}|\theta_{11}|^2 3\frac{f_{11}^2\omega_1^2}{g}r_{11q}\right.\\ & \left.+\theta_{11}|\theta_{12}|^2\left(2\frac{f_{12}^2\omega_2^2}{g}r_{11q}+4\frac{f_{12}\omega_2f_{11}\omega_1}{g}r_{12q}\right)\right],\end{aligned} \tag{B 5}$$

and

$$\begin{aligned}\mathcal{D}_{32}^{\pm} = & -\rho\int_{(q-1)a}^{qa}\mathrm{d}y\left\{\int_{-h_p}^{0}\mathrm{d}z\,[-6f_{12}r_{12q}^2\theta_{12}|\theta_{12}|^2\omega_2-6f_{11}r_{11q}\theta_{12q}\theta_{12}|\theta_{11}|^2\omega_1\right.\\ & -4f_{12}r_{11q}^2\theta_{12}|\theta_{11}|^2\omega_1-2\mathrm{i}f_{12}\theta_{12_t}](z+h_p)+\frac{f_{12}^3\omega_2^3}{g^2}\theta_{12}|\theta_{12}|^2+\frac{f_{11}^2\omega_1^2f_{12}\omega_2}{g^2}\theta_{12}|\theta_{11}|^2\\ & +2h_p\Delta\left[\frac{f_{11}\omega_1}{g}f_{24}(\omega_2-\omega_1)\theta_{12}|\theta_{11}|^2+\frac{f_{11}\omega_1}{g}f_{23}(\omega_2+\omega_1)\theta_{12}|\theta_{11}|^2\right.\\ & \left.+\ 2\frac{f_{12}\omega_2}{g}f_{22}\omega_2\theta_{12}|\theta_{12}|^2\right]-Ah_p(\omega_1+\omega_2)\Delta\left(\pm\frac{f_{11}\omega_1}{g}\phi^{\pm A}\theta_{11}^*\right)\Bigg\}+2\omega_1Ir_{12q}\mathrm{i}\theta_{12_t}\\ & +2\rho d\int_{(q-1)a}^{qa}\mathrm{d}y\int_{-h_p}^{0}\mathrm{d}z\,(\theta_{12}|\theta_{12}|^2 2\omega_2f_{22}r_{12q}+\theta_{12}|\theta_{11}|^2(\omega_1+\omega_2)f_{23}r_{11q}\\ & +\theta_{12}|\theta_{11}|^2(\omega_2-\omega_1)f_{24}r_{11q})+\rho\,d\int_{(q-1)a}^{qa}\mathrm{d}y\left[\theta_{12}|\theta_{12}|^2 3\frac{f_{12}^2\omega_2^2}{g}r_{12q}\right.\\ & \left.+\theta_{12}|\theta_{11}|^2\left(2\frac{f_{11}^2\omega_1^2}{g}r_{12q}+4\frac{f_{11}\omega_1f_{12}\omega_2}{g}r_{11q}\right)\right].\end{aligned} \tag{B 6}$$

REFERENCES

ADAMO, A. & MEI, C. C. 2005 Linear response of Venice storm gates to incident waves. *Proc. R. Soc. Lond.* A **461**, 1711–1734.

ALAM, M.-R. 2012 A new triad resonance between co-propagating surface and interfacial waves. *J. Fluid Mech.* **691**, 267–278.

ARANSON, I. & KRAMER, L. 2002 The world of the complex Ginzburg–Landau equation. *Rev. Mod. Phys.* **74** (1), 99C143.

BABARIT, A., HALS, J., MULIAWAN, M. J., KURNIAWAN, A., MOAN, T. & KROKSTAD, J. 2012 Numerical benchmarking study of a selection of wave energy converters. *Renew. Energy* **41**, 44–63.

BLONDEAUX, P. & VITTORI, G. 1995 The nonlinear excitation of synchronous edge waves by a monochromatic wave normally incident on a plane beach. *J. Fluid Mech.* **301**, 251–268.

CILIBERTO, S. & GOLLUB, J. P. 1985 Chaotic mode competition in parametrically forced surface waves. *J. Fluid Mech.* **158**, 381–398.

EVANS, D. V. & LINTON, C. M. 1991 Trapped modes in open channels. *J. Fluid Mech.* **225**, 153–175.

FOLLEY, M., WHITTAKER, T. & VAN'T HOFF, J. 2007 The design of small seabed mounted bottom-hinged wave energy converters. In *Proceedings of the 7th European Wave and Tidal Energy Conference, Porto, Portugal, 2007*.

GU, X. M. & SETHNA, P. R. 1987 Resonant surface waves and chaotic phenomena. *J. Fluid Mech.* **183**, 543–565.

GUCKENHEIMER, J. & HOLMES, P. 1983 *Nonlinear Oscillations, Dynamical Systems and Bifurcation of Vector Fields*. Springer.

GUZA, R. T. & BOWEN, A. J. 1976 Finite amplitude Stokes edge waves. *J. Mar. Res.* **34**, 269–293.

HEIN, S. & KOCH, W. 2008 Acoustic resonances and trapped modes in pipes and tunnels. *J. Fluid Mech.* **605**, 401–428.

HENRY, A., DOHERTY, K., CAMERON, L., WHITTAKER, T. & DOHERTY, R. 2010 Advances in the design of the oyster wave energy converter. In *Marine Renewables and Offshore Wind Conference, Royal Institute of Naval Architects, London, 2010*.

HOLMES, P. 1986 Chaotic motion in a weakly nonlinear model for surface waves. *J. Fluid Mech.* **162**, 365–388.

JORDAN, D. W. & SMITH, P. 2011 *Nonlinear Ordinary Differential Equations*. Oxford University Press.

KADRI, U. & AKYLAS, T. R. 2016 On resonant triad interactions of acoustic-gravity waves. *J. Fluid Mech.* **788**, R1.

KADRI, U. & STIASSNIE, M. 2013 Generation of an acoustic-gravity wave by two gravity waves, and their subsequent mutual interaction. *J. Fluid Mech.* **735**, R6.

KAMBE, T. & UMEKI, M. 1990 Nonlinear dynamics of two-mode interactions in parametric excitation of surface waves. *J. Fluid Mech.* **212**, 373–393.

LI, G. 2007 Nonlinear resonance of trapped waves on a plane beach. PhD thesis, Massachussetts Institute of Technology.

LI, G. & MEI, C. C. 2003 Natural modes of mobile flood gates. *Appl. Ocean Res.* **25**, 115–126.

LI, Y. & MEI, C. C. 2006 Subharmonic resonance of a trapped wave near a vertical cylinder in a channel. *J. Fluid Mech.* **561**, 391–416.

LICHTER, S. & CHEN, J. 1987 Subharmonic resonance of nonlinear cross-waves. *J. Fluid Mech.* **183**, 451–465.

LINTON, C. & MCIVER, P. 2001 *Mathematical Techniques for Wave/Structure Interactions*. Chapman & Hall/CRC.

LINTON, C. M. & RATCLIFFE, K. 2004 Bound states in coupled guides. I. Two dimensions. *J. Math. Phys.* **45**, 1359–1379.

MEI, C. C., SAMMARCO, P., CHAN, E. & PROCACCINI, C. 1994 Subharmonic resonance of proposed storm Venice gates for Venice lagoon. *Proc. R. Soc. Lond.* A **444**, 257–265.

MEI, C. C., STIASSNIE, M. & YUE, D. K.-Y. 2005 *Theory and Application of Ocean Surface Waves*. World Scientific.

MEI, C. C. & ZHOU, X. 1991 Parametric resonance of a spherical bubble. *J. Fluid Mech.* **229**, 29–50.

MICHELE, S., SAMMARCO, P. & D'ERRICO, M. 2016*a* The optimal design of a flap gate array in front of a straight vertical wall: resonance of the natural modes and enhancement of the exciting torque. *Ocean Engng* **118**, 152–164.

MICHELE, S., SAMMARCO, P. & D'ERRICO, M. 2016*b* Theory of the synchronous motion of an array of floating flap gates oscillating wave surge converter. *Proc. R. Soc. Lond.* A **472**, 20160174.

MICHELE, S., SAMMARCO, P., D'ERRICO, M., RENZI, E., ABDOLALI, A., BELLOTTI, G. & DIAS, F. 2015 Flap gate farm: from Venice lagoon defense to resonating wave energy production. Part 2: synchronous response to incident waves in open sea. *Appl. Ocean Res.* **52**, 43–61.

MILES, J. 1984*a* Nonlinear Faraday resonance. *J. Fluid Mech.* **146**, 285–302.

MILES, J. & HENDERSON, D. 1990 Parametrically forced surface waves. *Annu. Rev. Fluid Mech.* **22**, 143–165.

NAYFEH, A. H. & MOOK, D. T. 1995 *Nonlinear Oscillations*. Wiley Classic Library.

PORTER, R. 2007 Trapped modes in thin elastic plates. *Wave Motion* **45**, 3–15.

PORTER, R. & EVANS, D. V. 1999 Rayleigh–Bloch surface waves along periodic gratings and their connection with trapped modes in waveguides. *J. Fluid Mech.* **386**, 233–258.

RENZI, E. & DIAS, F. 2012 Resonant behaviour of an oscillating wave energy converter in a channel. *J. Fluid Mech.* **701**, 482–510.

RENZI, E. & DIAS, F. 2013 Hydrodynamics of the oscllating wave surge converter in the open ocean. *Eur. J. Mech. (*B*/Fluids)* **41**, 1–10.

RENZI, E. & DIAS, F. 2014 Motion resonant modes of large articulated damped oscillators in waves. *J. Fluids Struct.* **49**, 705–715.

ROCKLIFF, N. 1978 Finite amplitude effects in free and forced edge waves. *Math. Proc. Camb. Phil. Soc.* **83**, 463–479.

SAMMARCO, P., MICHELE, S. & D'ERRICO, M. 2013 Flap gate farm: from Venice lagoon defense to resonating wave energy production. Part 1: natural modes. *Appl. Ocean Res.* **43**, 203–213.

SAMMARCO, P., TRAN, H. H., GOTTLIEB, O. & MEI, C. C. 1997*b* Subharmonic resonance of Venice gates in waves. Part 2. Sinusoidally modulated incident waves. *J. Fluid Mech.* **349**, 327–359.

SAMMARCO, P., TRAN, H. H. & MEI, C. C. 1997*a* Subharmonic resonance of Venice gates in waves. Part 1. Evolution equation and uniform incident waves. *J. Fluid Mech.* **349**, 295–325.

SARKAR, D., DOHERTY, K. & DIAS, F. 2016 The modular concept of the oscillating wave surge converters. *Renew. Energy* **85**, 484–497.

SIMONELLI, F. & GOLLUB, J. P. 1989 Surface wave mode interactions: effects of symmetry and degeneracy. *J. Fluid Mech.* **199**, 471–494.

TRULSEN, K. & DYSTHE, K. B. 1997 Frequency downshift in three-dimensional wave trains in a deep basin. *J. Fluid Mech.* **352**, 359–373.

TRULSEN, K. & MEI, C. C. 1995 Modulation of three resonating gravity-capillary waves by a long gravity wave. *J. Fluid Mech.* **290**, 345–376.

UMEKI, M. 1991 Faraday resonance in rectangular geometry. *J. Fluid Mech.* **227**, 161–192.

VITTORI, G., BLONDEAUX, P. & SEMINARA, G. 1996 Waves of finite amplitude trapped by oscillating gates. *Proc. R. Soc. Lond.* A **452**, 791–811.

ZARDI, D. & SEMINARA, G. 1995 Chaotic mode competition in the shape of pulsating bubbles. *J. Fluid Mech.* **286**, 257–276.